



Mid-Atlantic US observations of radiocarbon in CO₂: fossil and biogenic source partitioning and model evaluation

Bianca C. Baier¹, John B. Miller¹, Colm Sweeney¹, Scott J. Lehman², Chad Wolak², Joshua P. DiGangi³,
Yonghoon Choi^{3,4}, Kenneth Davis^{5,6}, Sha Feng^{5,a}, and Thomas Lauvaux^{5,b}

¹NOAA Global Monitoring Laboratory, Boulder, CO 80305, USA

²Institute of Arctic and Alpine Research, University of Colorado-Boulder, Boulder, CO 80309, USA

³NASA Langley Research Center, Hampton, VA 23681, USA

⁴Analytical Mechanics Associated, Hampton, VA 23666, USA

⁵Department of Meteorology and Atmospheric Science, The Pennsylvania State University,
University Park, PA 16802, USA

⁶Earth and Environmental Systems Institute, The Pennsylvania State University,
University Park, PA 16802, USA

^anow at: Atmospheric, Climate and Earth Sciences Division, Pacific Northwest National Laboratory,
Richland, WA 99352, USA

^bnow at: Groupe de Spectrométrie Moléculaire et Atmosphérique (GSMA), Université de Reims-Champagne
Ardenne, UMR CNRS 7331, 51100 Reims, France

Correspondence: Bianca C. Baier (bianca.baier@noaa.gov)

Received: 20 February 2025 – Discussion started: 10 March 2025

Revised: 26 June 2025 – Accepted: 27 June 2025 – Published: 15 September 2025

Abstract. Accurately quantifying regional anthropogenic CO₂ fluxes is fundamental to improving our understanding of the carbon cycle and for creating effective carbon mitigation policies, and the radiocarbon to total carbon ratio in atmospheric CO₂ ($\Delta^{14}\text{CO}_2$) is a robust tracer of fossil fuel CO₂ that can discriminate between biogenic and fossil fuel CO₂ sources. NASA's Atmospheric Carbon and Transport-America (ACT-America) airborne mission between 2016 and 2019 aimed to improve the accuracy of regional greenhouse gas flux estimates, through refining our understanding and characterization of fluxes and flux uncertainties in models. $\Delta^{14}\text{CO}_2$ observations from 26 flights are presented for examining seasonal CO₂ source partitioning in the Mid-Atlantic USA. Observed variability in boundary layer CO₂ at timescales ranging from intra-day to seasonal was largely driven by biogenic CO₂ (CO_{2bio}) variability that ranged from -19.7 ppm in summer to 16.2 ppm in fall, while fossil fuel CO₂ (CO_{2ff}) variability remained at 3.3 ± 2.0 ppm. Carbonyl sulfide uptake was well-correlated with CO_{2bio} uptake, and examining this relationship, as well as that between CO₂ and CO_{2bio} variability reinforces the seasonal extent of gross primary productivity response throughout ACT-America. We use airborne $\Delta^{14}\text{CO}_2$ flask sampling alongside in situ carbon monoxide measurements to calculate high-frequency CO_{2ff} and evaluate the magnitude and diurnal variability of modeled CO_{2ff}, deducing likely transport errors in an example flight. Although ACT-America CO_{2ff} signals were attenuated due to the broad source regions sampled, results illustrate the value of $\Delta^{14}\text{CO}_2$ sampling and observation-based methodologies for regional CO₂ flux attribution, evaluation and improvement of modeled CO₂.

1 Introduction

Anthropogenic carbon dioxide (CO₂) emissions have driven more than a 50 % increase in atmospheric CO₂ abundances globally since pre-industrial levels, despite almost half of these emissions being removed from the atmosphere by terrestrial and oceanic reservoirs (i.e., “sinks”; Ballantyne et al., 2012; Friedlingstein et al., 2022). Because total CO₂ fluxes encompass biogenic, oceanic and anthropogenic processes and because regional spatial scales are ones at which carbon mitigation strategies are generally developed and implemented, it is important that these CO₂ component processes be accurately quantified. Fossil fuel emissions represent the bulk of the net atmospheric CO₂ flux annually on regional scales for North America (King et al., 2007; USGCRP, 2018). However, while national-scale fossil fuel CO₂ fluxes for many countries are likely known to within 10 % (Gregg et al., 2009; Andres et al., 2012), fluxes and their variability are less certain on smaller spatial and temporal scales (USGCRP, 2018; Gurney et al., 2021). Even so, fossil fuel fluxes are currently reported with uncertainties up to 5 times lower than biospheric CO₂ fluxes on regional scales (Hayes et al., 2012; King et al., 2015; USGCRP, 2018).

Atmospheric CO₂ and its long-term global growth rate can be directly determined from in situ observations, because observed CO₂ over large land areas is a function of both fossil fuel emissions and net ecosystem exchange (NEE) with the terrestrial biosphere. Distinguishing fossil fuel from biogenic CO₂ fluxes cannot be accomplished from CO₂ observations alone (Shiga et al., 2014; Basu et al., 2016). The radiocarbon to total carbon ratio in atmospheric CO₂ (¹⁴C:C, expressed as Δ¹⁴CO₂) has been demonstrated to be a robust and largely unbiased tracer for accurately constraining recently emitted fossil fuel CO₂ (CO_{2ff}) into the atmosphere because fossil fuels do not contain ¹⁴C (Levin et al., 2003; Levin and Karstens, 2007; Graven et al., 2009; Vogel et al., 2010; Miller et al., 2012; Turnbull et al., 2006, 2011a, b, 2015). By isolating this fossil fuel component and its variability relative to background levels, the remaining variability in CO₂ can be attributed to biogenic processes.

Inverse models using only CO₂ measurements can theoretically be used to disaggregate anthropogenic and biogenic CO₂ fluxes when these emissions can be adequately separated in time and space, but given the low density of most regional measurement networks, fossil and biogenic fluxes are colocated, so this disaggregation cannot be achieved in practice (Shiga et al., 2014; Basu et al., 2016). In many situations from regional to global scales, prior fossil CO₂ emissions are traditionally pre-specified and not optimized in CO₂ measurement-based inversions (Gurney et al., 2003; Ciais et al., 2010; Schuh et al., 2010; Lauvaux et al., 2012) on the basis that fossil fluxes are much better known than terrestrial biospheric fluxes. Much work has been done to characterize model uncertainty and improve estimates of CO₂. At the continental scale and for annual time frames, Feng et

al. (2019a) used a forward-calibrated model ensemble (Feng et al., 2019b) to show that the uncertainty in simulated North American atmospheric CO₂ mole fractions comes primarily from two approximately equivalent sources: fossil fuel emissions and biogenic CO₂ fluxes. At these timescales, these two sources greatly outweighed the uncertainty contributions from atmospheric transport and from continental boundary conditions, and Feng et al. (2019a) note that accurate accounting of fossil fuel emissions uncertainties in models can further improve regional biospheric flux estimates. Brophy et al. (2019) emphasized the need for varying prior fossil fuel emissions estimates in time, alongside needed improvements in the representation of atmospheric transport to accurately represent CO₂ fluxes at approximately sub-annual and regional scales. Modelers have also relaxed the assumption of perfectly known fossil CO₂ emissions – and have lowered fossil fuel emissions uncertainties – by assimilating Δ¹⁴CO₂ measurements (or CO_{2ff}) alongside CO₂ and carefully controlling systematic model errors and errors in prior flux estimates (Basu et al., 2016, 2020; Fischer et al., 2017).

Using aircraft Δ¹⁴CO₂ observations, an effort has been made to evaluate modeled CO_{2ff} and to estimate or verify regional emissions inventories (e.g., Graven et al., 2009; Basu et al., 2020). At the urban scale, studies have also successfully used Δ¹⁴CO₂ measurements alongside in situ carbon monoxide (CO) observations from surface- and aircraft-based platforms to calculate high-resolution proxy estimates of recently added CO_{2ff} to the atmosphere, given well-characterized CO:CO_{2ff} ratios (Vogel et al., 2010; Turnbull et al., 2011a, 2019; Lauvaux et al., 2020; Wu et al., 2022). As biogenic CO₂ emissions and sinks – even within cities – are non-negligible and as ignoring these signals could potentially bias fossil fuel CO₂ emissions inventories, Δ¹⁴CO₂ measurements play an important role in determining biogenically driven (CO₂ photosynthesis and respiration) emissions or sinks (Levin et al., 2003; Lopez et al., 2013; Turnbull et al., 2015; Miller et al., 2020). One tracer that could aid in the understanding of CO₂ uptake processes alongside Δ¹⁴CO₂ is carbonyl sulfide (OCS), which is taken up by plants but not respired (Montzka et al., 2007; Campbell et al., 2008).

NASA's multi-year Atmospheric Carbon and Transport (ACT)-America Earth Venture Suborbital mission was directed toward improving the accuracy of regional greenhouse gas flux estimates, specifically through refining our understanding and implementation of CO₂ and methane (CH₄) transport, fluxes and flux uncertainties, and background levels in inverse models (Davis et al., 2021). During this mission, five seasonal research flight campaigns were conducted between 2016 and 2019 for evaluation and subsequent improvement of terrestrial carbon cycle models and for filling gaps in the eastern US carbon monitoring network. With a strong focus on transport of carbon via weather systems, atmospheric trace gases and meteorological variables were also observed across multiple synoptic cycles, across cold and warm air sectors, and from the boundary layer to the

upper troposphere. While the ACT mission was not targeting large carbon emissions signals in urban areas as in the abovementioned studies, we focus on carbon flux attribution and model evaluation here. We analyze a spatially dense set of airborne whole-air flask $\Delta^{14}\text{CO}_2$ measurements collected during ACT in the Mid-Atlantic USA alongside those of other gas-phase species such as OCS, a tracer for photosynthetic uptake of CO₂, to first distinguish between biogenically driven and fossil fuel atmospheric CO₂ variability relative to background levels. Second, we apply the methodology of previous authors (Levin and Karstens, 2007; Vogel et al., 2010; Turnbull et al., 2011a; Maier et al., 2024a) to the broad Mid-Atlantic US region, calculating high-frequency fossil fuel CO₂ enhancements using in situ CO observations, and we investigate the utility of this technique for evaluating modeled atmospheric fossil fuel CO₂ enhancements above background levels for an example ACT research flight along the northeastern corridor.

2 Data and methods

2.1 ACT-America flight campaigns

During the ACT mission, the eastern half of the coterminous USA was broadly surveyed by two research aircraft: the NASA Langley Beechcraft B-200 King Air and the NASA Wallops C-130 Hercules. Of the Mid-Atlantic, Midwestern and Southern US-focused measurement regions, air samples for $\Delta^{14}\text{CO}_2$ measurement were collected only in the Mid-Atlantic region due to proximity to the northeastern US urban corridor and likelihood for higher $\Delta^{14}\text{CO}_2$ signals. Sampling in the Mid-Atlantic region focused heavily on the extensive forests and croplands with flights capturing distant urban influence, and a few selected flights specifically targeted the urban northeastern corridor. The first ACT campaign occurred during summer 2016 (18 July–28 August) and is omitted from this analysis due to the absence of $\Delta^{14}\text{CO}_2$ sampling. Four subsequent ACT campaigns described here occurred during winter 2017 (1–10 March), fall 2017 (1–15 October), spring 2018 (4–20 May) and summer 2019 (7–27 July) for a total of 26 flights with atmospheric sampling for $\Delta^{14}\text{CO}_2$. Research flights were primarily conducted between 11:00 and 18:00 LT (local time) to sample a well-developed atmospheric boundary layer (ABL), through long, level-leg flight transects. Airborne atmospheric sampling during individual research flights was focused at altitudes within the ABL (flight altitudes of 330 m a.g.l. (above ground level) in most cases) where greenhouse gas abundances are strongly influenced by surface fluxes with occasional sampling in the free troposphere (FT, ~ 2400 to 9000 m a.m.s.l. (above mean sea level)) to determine chemistry and isotopic composition of background air against which observed ABL enhancements or depletions are assumed to occur. Because a scientific goal of ACT was to improve the simulation of atmospheric transport of greenhouse gases in regional-scale in-

versions under real-world conditions, research flights were organized to sample across synoptic weather patterns (Pal et al., 2020). Wei et al. (2021) describe the ACT observational and numerical data products.

2.2 Whole-air sample collection and flask radiocarbon measurements

NOAA Programmable Flask Packages (PFPs) were installed on each aircraft for the collection of whole-air samples. Each PFP contains twelve 0.7 L borosilicate glass flasks, and for ACT campaigns between 2017 and 2019 these automated systems were connected to a Peltier gas chiller to efficiently dry air samples to less than 1 % atmospheric water vapor prior to air sample collection. Flask-filling times varied between 2 (ABL) to 4 min (FT), depending on the altitude of the aircraft. A Programmable Compressor Package (PCP) pressurized each flask to 275 kPa, yielding ~ 2 L of air at standard temperature and pressure conditions collected per flask. The technical details of these flask sampling systems used during ACT are described in Baier et al. (2020).

For each flight day, roughly 6 to 18 total flasks were filled on each aircraft platform between the altitudes of 300–9000 m a.m.s.l. The ratio of well-mixed ABL to FT flasks sampled during ACT was generally 5 : 1. Because approximately 2 L of sample air is required for high-precision $\Delta^{14}\text{CO}_2$, in addition to the long-lived greenhouse gases (CO₂, CH₄) and other low concentration gases such as OCS and CO, two PFP flasks were filled in parallel (i.e., “paired sampling”) when sampling for $\Delta^{14}\text{CO}_2$ measurements. Post-flight, PFPs were transferred to the NOAA Global Monitoring Laboratory and the University of Colorado INSTAAR Stable Isotope Laboratory for measurement. The first flask of each paired sample was analyzed for greenhouse gases; OCS; and a suite of hydrocarbons, halocarbons, and stable isotope ratios (^{13}C : ^{12}C) of CO₂ and methane using methods described in Baier et al. (2020), online (<https://gml.noaa.gov/ccgg/aircraft/analysis.html>, last access: 5 November 2024), and in Vaughn et al. (2004). Remaining sample air in the first flask after these measurements was combined with the entire second paired flask for a single $\Delta^{14}\text{CO}_2$ measurement. The University of Colorado INSTAAR Laboratory for AMS Radiocarbon Preparation and Research (NSRL) conducts the CO₂ extraction from flask sample air. Pure CO₂ is archived until near the time of $\Delta^{14}\text{CO}_2$ measurement, at which time the pure CO₂ is graphitized to pure carbon “targets”, and these graphitized samples are transferred to the University of California at Irvine for high-count accelerator mass spectrometry (AMS) ^{14}C measurement (Turnbull et al., 2007; Lehman et al., 2013). In total, 380 $^{14}\text{CO}_2$ samples were analyzed throughout the ACT campaigns: 87 in winter 2017, 100 in fall 2017, 104 in spring 2018 and 89 in summer 2019.

2.3 Radiocarbon-based CO₂ partitioning

Radiocarbon (¹⁴C) is produced naturally in the troposphere and stratosphere via cosmic-ray-induced reactions between neutrons and atmospheric nitrogen (N₂) (Libby, 1946). Measurements are presented as Δ¹⁴CO₂ in units of per mill (‰), i.e., the part per thousand deviation of the measured ¹⁴C : C ratio from that of the international measurement standard material, after correction for mass-dependent fractionation and radioactive decay since the date of collection (Stuiver and Polach, 1977). Given that the ¹⁴C half-life is approximately 5730 years (Godwin, 1962) and that fossil fuel carbon has been isolated from the atmosphere for millions of years, the radiocarbon content of fossil fuels is zero; therefore, Δ¹⁴CO_{2ff} is −1000 ‰ on the delta (Δ) scale. Therefore, addition of fossil fuel CO₂ to the atmosphere produces a quantitative reduction in atmospheric Δ¹⁴CO₂ over and downwind of emissions sources. Paired observations of Δ¹⁴CO₂ and CO₂ in flasks sampled in the Mid-Atlantic region can thereby provide a robust method for distinguishing between terrestrial biogenic (CO_{2bio}) and fossil fuel (CO_{2ff}) CO₂ sources, given a known background. The CO₂ mass balance over land is

$$\text{CO}_{2\text{obs}} = \text{CO}_{2\text{bg}} + \text{CO}_{2\text{ff}} + \text{CO}_{2\text{bio}}. \quad (1)$$

Expanding CO_{2bio}, which results from net ecosystem exchange, into a sum of photosynthetic (*photo*) and respiration (*resp*) fluxes (CO_{2resp} + CO_{2photo}) and adding the respective isotopic signatures (“Δ”, for Δ¹⁴CO₂) for all terms gives Eq. (2):

$$\begin{aligned} \Delta_{\text{obs}} \text{CO}_{2\text{obs}} &= \Delta_{\text{bg}} \text{CO}_{2\text{bg}} + \Delta_{\text{ff}} \text{CO}_{2\text{ff}} + \Delta_{\text{resp}} \text{CO}_{2\text{resp}} \\ &+ \Delta_{\text{photo}} \text{CO}_{2\text{photo}} + N^{14}C_{\text{nuc}}/R_{\text{std}}, \end{aligned} \quad (2)$$

where the individual budget terms are the product of the isotopic ratio and CO₂ mole fraction, which is a conserved quantity (Tans et al., 1993). Here, “obs” is the observed atmospheric mole fraction of CO₂ in the ABL and is a function of variations in fossil fuel (ff) and biogenic (bio) CO₂ differences from a varying CO₂ background (bg) level. We note that an oceanic term is sometimes written in Eq. (1), but we assume that the dominant oceanic CO₂ influence is encompassed in the background (bg) term. Photosynthesis and respiration contributions are stated separately in the isotopic mass balance (Eq. 2), because they carry different isotopic signatures. This isotopic “disequilibrium” between photosynthetic and respiration fluxes arises from the rapidly decreasing (∼ −5 ‰ yr^{−1}) background Δ¹⁴CO₂ (e.g., Lehman et al., 2013; Graven et al., 2020). Δ_{resp} is more positive than Δ_{photo}, because Δ_{resp} is associated with biospheric CO₂ fixed by photosynthesis when the ambient atmospheric Δ¹⁴CO₂ (i.e., Δ_{bg}) was higher. Δ_{photo} is assumed equal to Δ_{bg}, because the “Δ” notation accounts for mass-dependent fractionation processes such as those occurring during photosynthesis. Turnbull et al. (2009) note that this

assumption is valid in the limit that time and space between background and observation tends to zero. There is also a small impact on Δ_{obs} from pure ¹⁴C emitted from certain nuclear reactors, which is added as the last term in Eq. (2) (Graven and Gruber, 2011). Because this term is significantly smaller than all other terms in Eq. (1), it is omitted there. Here *N* is the mass-dependent Δ normalization factor, which is close to 1 (Basu et al., 2016), ¹⁴C_{nuc} is the mole fraction of Δ¹⁴CO₂ resulting from the ¹⁴C flux from reactors, and *R*_{std} is the standard material ¹⁴C / C ratio.

Combining Eqs. (1) and (2) results in

$$\begin{aligned} \text{CO}_{2\text{ff}} &= \frac{\text{CO}_{2\text{obs}} (\Delta_{\text{obs}} - \Delta_{\text{bg}})}{(\Delta_{\text{ff}} - \Delta_{\text{bg}})} - \frac{\text{CO}_{2\text{resp}} (\Delta_{\text{resp}} - \Delta_{\text{bg}})}{(\Delta_{\text{ff}} - \Delta_{\text{bg}})} \\ &- N^{14}C_{\text{nuc}}/R_{\text{std}}/(\Delta_{\text{ff}} - \Delta_{\text{bg}}). \end{aligned} \quad (3)$$

The variables in Eq. (3) are either known or can be measured or calculated directly. Historically, CO_{2ff} has been approximated by only the first term on the right-hand side of Eq. (3) (Levin et al., 2003). Disequilibrium and nuclear fluxes both add ¹⁴C to the atmosphere. A correction (CO_{2corr}) is made to CO_{2ff} (Turnbull et al., 2009) to unmask these effects and reveal the full magnitude of the fossil fuel CO₂ emissions signal, making it somewhat convenient to rewrite Eq. (3) as

$$\text{CO}_{2\text{ff}} = \frac{\text{CO}_{2\text{obs}} (\Delta_{\text{obs}} - \Delta_{\text{bg}})}{(\Delta_{\text{ff}} - \Delta_{\text{bg}})} - \text{CO}_{2\text{corr}}. \quad (4)$$

Flask ABL measurements for CO_{2obs} are defined as those samples collected at altitudes less than 1500 m a.m.s.l. for all ACT flight campaigns. ABL samples typically contain the strongest regional flux signatures; thus, are likely to yield the largest Δ¹⁴C signals. Conversely, we determine daily Δ_{bg} and CO_{2bg} values from measurements of ¹⁴CO₂ and CO₂ in flasks sampled at altitudes greater than 4000 m a.m.s.l. for all flight campaigns to capture air that is within the well-mixed FT in all seasons. The FT data, while perhaps not always representative of the true local-scale background signature (e.g., Turnbull et al., 2015), are expected to provide a reliable estimate of the regional- to continental-scale background (Baier et al., 2020). Here, Δ_{bg} in Eq. (2) is derived as the daily mean FT Δ¹⁴CO₂, typically between 4000 and 9000 m a.m.s.l. All flask FT measurements are filtered to remove samples with high CO (above 3 standard deviations from a smooth curve fit), which can indicate the potential influence of local pollution on continental background values. Similarly, CO_{2bg} and other trace gas background mole fractions were derived as mean mole fractions of FT values for these species. For the ACT study, CO_{2corr} is derived for each flask sample by convolving estimated gridded monthly disequilibrium fluxes of Δ¹⁴CO₂ from the terrestrial biosphere and fluxes from nuclear reactors with surface influence functions for each flask sample location (i.e., for each flask “receptor”, as per below).

Surface influence functions (referred to as “footprints”), representing the sensitivity of air parcels at a particu-

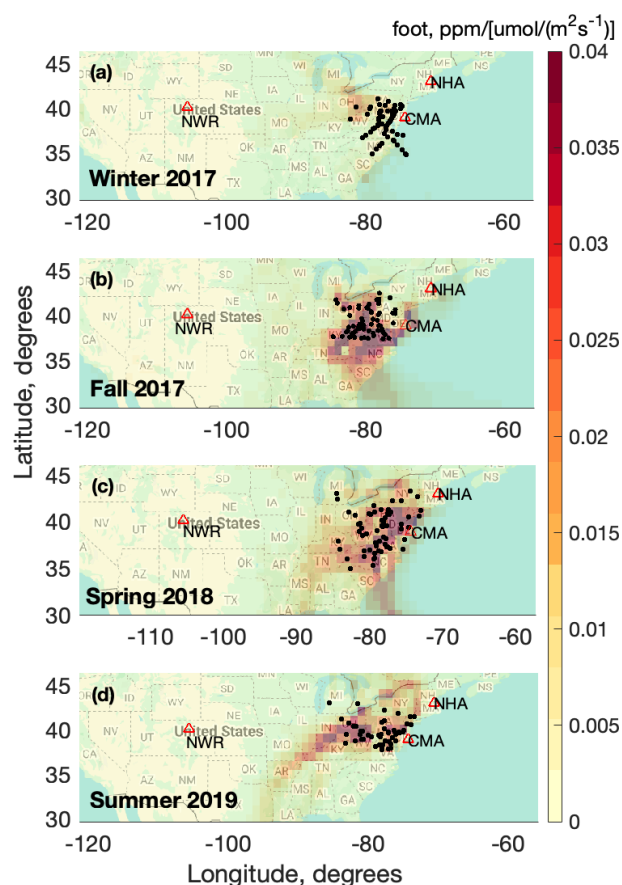


Figure 1. Surface influence for ABL $\Delta^{14}\text{CO}_2$ samples measured for ACT seasonal deployments in (a) winter 2017, (b) fall 2017, (c) spring 2018 and (d) summer 2019. ABL flask sample locations are denoted in black, with GGGRN aircraft program network sites indicated at Niwot Ridge, CO (NWR); Cape May, NJ (CMA); and Portsmouth, NH (NHA). Plot maps are produced using Google Maps API (© Google Maps 2025).

lar receptor location to upwind surface fluxes (in units of $\text{ppm m}^2 \text{s} \mu\text{mol}^{-1}$), are derived by first using the Hybrid Single-Particle Lagrangian Integrated Trajectory (HYSPLIT) model (Stein et al., 2015), running 500 randomly perturbed, 10 d back-trajectories for all ABL flask receptors. Back-trajectories are driven by 27 km horizontal resolution Weather Research and Forecasting (WRF) meteorological fields, nudged to the ERA-5 reanalysis meteorology within the ACT-America North American model domain (Feng et al., 2021b; see Sect. 2.4). Individual footprints are calculated for all 500-particle trajectory ensemble members based on their residence time over a given gridded area (Lin et al., 2003) within the surface boundary, defined as a vertical column of air in each $1^\circ \times 1^\circ$ grid cell between 125 m a.g.l. and 50 % of the WRF-calculated atmospheric boundary layer height (Fig. 1). Referring to Eqs. (1) and (2), though there exists a footprint signature on flask samples during fall 2017 and spring 2018, this influence is relatively small. Disequi-

librium fluxes from the terrestrial biosphere are derived by convolving impulse-response functions from the CASA biogeochemical model (Thompson and Randerson, 1999) with the atmospheric history of ^{14}C (Miller et al., 2012; LaFranchi et al., 2013; with updates in Zhou et al., 2020), while nuclear reactor fluxes are obtained from Graven and Gruber (2011), effectively assuming regional nuclear $^{14}\text{CO}_2$ has not changed significantly over time through 2019. These gridded fluxes (monthly, time-dependent in the case of disequilibrium flux) are converted to the two components of $\text{CO}_{2\text{corr}}$ via convolution with footprints derived from HYSPLIT and are calculated individually for each ABL flask sample pair for which $\text{CO}_{2\text{ff}}$ is derived using Eq. (4). We note that the calculated magnitude of $\text{CO}_{2\text{corr}}$ attributable to nuclear reactor emissions in the Mid-Atlantic USA is $0.25 \pm 0.44 \text{ ppm CO}_2$ and does not exhibit a seasonal pattern as it is assumed constant annually. Graven and Gruber (2011) data have been used at the time that this publication was written, but updates to nuclear reactor fluxes have been published in Zazzeri et al. (2023). The magnitude of $\text{CO}_{2\text{corr}}$ attributable to the terrestrial biosphere in the Mid-Atlantic USA is approximately $0.10 \pm 0.04 \text{ ppm CO}_{2\text{ff}}$ (1σ) during the winter deployment and exhibits a seasonal cycle with a maximum during the summer of $0.70 \pm 0.28 \text{ ppm CO}_{2\text{ff}}$ (1σ), indicating similar seasonal behavior as that calculated by Miller et al. (2012) for the Mid-Atlantic USA. In total, the average magnitude of $\text{CO}_{2\text{corr}}$ ($0.8 \pm 0.6 \text{ ppm}$) calculated here to correct $\text{CO}_{2\text{ff}}$ in this work is roughly comparable that first described in Turnbull et al. (2006).

2.4 Forward model $\text{CO}_{2\text{ff}}$ using the PSUWRF model

A separate Eulerian 27 km horizontal resolution implementation of WRF-Chem version 3.6.1 run (Feng et al., 2021a, b) was implemented by The Pennsylvania State University (hereby called PSUWRF) with 50 vertical levels from the surface to 50 hPa, with 29 of these vertical levels in the lowermost 2 km. PSUWRF was developed and implemented during the ACT time period (2016–2019) to simulate atmospheric transport of CO_2 component fluxes along all flight tracks for each seasonal campaign. Note that while the Lagrangian HYSPLIT model mentioned above to calculate $\text{CO}_{2\text{corr}}$ in Eq. (4) for each flask measurement also used WRF for input meteorological fields, this was not identical to PSUWRF that was used for the Eulerian simulations. PSUWRF model runs were implemented prior to this paper development and could not be rerun, but both WRF versions used similar setups; thus, we expect there to be no major inconsistencies between the use of these two different versions for calculating $\text{CO}_{2\text{ff}}$ using flask or model output.

PSUWRF separately simulates the contributions of CO_2 boundary conditions and biogenic, ocean, fossil fuel, and biomass burning CO_2 fluxes to total CO_2 at any time and location in the model domain (Feng et al., 2019a, b). The microphysics, planetary boundary layer and cumu-

lus parameterization schemes used in this run are Thompson microphysics, the Mellor–Yamada–Nakanishi–Nino version 2 (MYNN2) and the Kain–Fritsch schemes, respectively (Feng et al., 2019a). As the ACT campaigns spanned multiple years, CO₂ oceanic, fossil fuel and biomass burning fluxes, as well as total CO₂ boundary conditions, come from CarbonTracker version 2017 (CT2017) through 2017 and CT-NRTv2019-2 (Jacobson et al., 2020) afterwards. CT2017 and CT-NRTv2019-2 together are called “CT” for simplicity. The CT fossil fuel tracer typically is derived from an average of the ODIAC (Oda et al., 2018) and Miller emissions datasets. As both datasets have very similar global and national fossil fuel emissions totals but include differences in spatial and temporal emissions distributions, an average of the two is used in CT to optimize the mapping of these emissions (Jacobson et al., 2020). In PSUWRF, ODIAC and Miller datasets were run separately for initial model runs between 2016–2018 to experimentally investigate potential differences between the two; however, only small differences within ~ 2 ppm CO_{2ff} are seen between the two and are not expected to create inconsistencies in CO_{2ff} simulated by PSUWRF between 2016–2019. As such, ODIAC and Miller are averaged to create a single flux product and to simplify model runs as in CT for 2019. In PSUWRF, simulated fossil fuel CO₂ (CO_{2ffmod}) is calculated using the same approach as flask CO_{2ff}, where average FT values of this tracer are subtracted from ABL values. The PSUWRF model transport is nudged to ERA5 reanalysis data to improve the depiction of atmospheric transport relative to ACT in-flight meteorological observations (Gerken et al., 2021). The PSUWRF model output was extracted to ACT research flight track locations at hourly resolution for comparison and evaluation relative to high-frequency measurement-based CO_{2ff} described in Sect. 2.5.

2.5 Calculation of “pseudo-CO_{2ff}”

As in previous studies (Levin and Karstens, 2007; Vogel et al., 2010; Turnbull et al., 2011a; Maier et al., 2024a), we employ in situ CO measurements for estimating CO_{2ff} (referred to as “pseudo-CO_{2ff}” and denoted as CO_{2ff}') at high temporal resolution. ACT in situ CO measurements were made by cavity ring-down spectroscopy at 0.4 Hz, drift-corrected during flight and calibrated once weekly using gas standards on the World Meteorological Organization (WMO) X2014A CO scale, same as NOAA flask-based measurements (Wei et al., 2021; DiGangi et al., 2021). After calibration, CO data were averaged to 0.2 Hz, i.e., the maximum frequency of CO_{2ff}'. We calculate CO_{2ff}' using Eq. (5) by applying a median ratio of CO to CO_{2ff} (R_{CO}) calculated strictly from flask samples collected each day (typically from 5–12 flask samples), and we apply this value to the in situ CO time series

collected on that day's ACT research flight:

$$CO_{2ff}' = \frac{CO_{obs}' - \overline{CO_{bg}'}}{R_{CO}}. \quad (5)$$

Here, CO_{obs}' represents 0.2 Hz ABL (below 1500 m a.m.s.l.) in situ CO dry mole fraction observations, and $\overline{CO_{bg}'}$ represents the mean daily CO mole fraction observed in the FT (above 4000 m a.m.s.l.) for each flight day. R_{CO} is calculated as the median value of all flask measurements each day, i :

$$R_{CO} = \frac{[CO_{obs,flask} - \overline{CO_{bg,flask}}]_i}{CO_{2ff,flask_i}}. \quad (6)$$

A median R_{CO} is used each day due to difficulty with respect to calculating seasonal regression slopes with low correlations (seasonal R^2 between 0.08–0.33) in the flask CO enhancement and CO_{2ff} data. In calculating daily median R_{CO} , it may be possible to capture some spatial variability of research flight observations rather than ignoring this variability and relying on average seasonal values. However, we acknowledge in Sect. 3.3.1 that this methodology, given low signal-to-noise ratio ($\Delta^{14}CO_2$ precision) in the ACT CO_{2ff} data, could create anomalous variability in R_{CO} and is one of the largest sources of uncertainty in this CO_{2ff}' calculation (as first presented in detail in Maier et al., 2024b) and a limitation to this analysis. In situ FT measurements are filtered to remove high CO or local emissions influences. Similar to the above, data with CO greater than 3 standard deviations from a smooth curve fit to background values are filtered. Each of these terms is derived exactly as the analysis of flask CO_{2ff} above. Due to the limited number of flasks sampled on each flight, R_{CO} is calculated as a daily median ratio of CO enhancements to CO_{2ff} from flask samples, and we assume that this ratio is representative of the entire flight region each day. In the analysis that follows, we assess the utility of this “pseudo-CO_{2ff}” method for determining fossil fuel CO₂ in evaluating modeled CO_{2ff} over larger regions where routine high-density discrete flask sampling is not available. In this work, CO_{2ff}' is calculated only for flights when flask measurements were sampled and analyzed for $\Delta^{14}CO_2$ in order to reduce errors associated with assumptions in R_{CO} spatial and temporal variability.

2.6 CO_{2ff} uncertainty derivation

The total estimated uncertainty in CO_{2ff} is determined by a propagation of estimated uncertainties for individual budget terms through Eq. (4). Flask-based CO_{2obs} and Δ_{obs} measurement uncertainties are 0.1 ppm and 1.8‰, respectively. Here Δ_{ff} is, by definition, -1000 ‰ and carries no uncertainty. The uncertainty in Δ_{bg} is calculated through propagation of error in (a) Δ_{obs} and (b) the mean diurnal standard deviation of FT $\Delta^{14}CO_2$ observations (Δ_{bg}) for each ACT flight. The relative uncertainty in CO_{2corr} associated with

biospheric disequilibrium and nuclear reactor fluxes is assumed to be 50 % for each term. Daily aggregated CO_{2ff} sample uncertainties are determined by using a 1000-member Monte Carlo simulation that propagates these uncertainties through Eq. (4) to provide an estimate of the flask-derived CO_{2ff} uncertainty per research flight. The average campaign-wide CO_{2ff} uncertainty (from the inner 68 % confidence interval of the 1000-member CO_{2ff} normal distribution per research flight) is 1.22 ppm.

Similar to the above, we calculate an average campaign uncertainty in CO_{2ff} of 4.96 ppm (from the inner 68 % confidence interval in CO_{2ff} of a 1000-member Monte Carlo approach for each flight day) using Eq. (5). We estimate daily uncertainties by conservatively incorporating the CO dry mole fraction measurement precision on 0.2 Hz measurements (5 ppb), the uncertainty in daily background CO from CO_{obs} and the daily standard deviation in FT CO, and the uncertainty in R_{CO} from the width of a normally distributed 68 % confidence interval about average R_{CO} values.

The uncertainty in both CO_{2ff} and CO_{2ff}' is higher for ACT research flights due to the uncertainty caused by using a single CO or $\Delta^{14}\text{CO}_2$ background value for each flight, when in truth different sectors of a research flight (e.g., the cold and warm sectors during frontal crossing flights) could experience different background conditions or could be influenced by deep convective mixing, violating the assumption that the continental background value is described by the FT value. Elevating the altitude threshold at which background values are defined (i.e., 4000 m a.m.s.l.) can better isolate continental background air from lower tropospheric air that has been mixed with local emissions sources. However, using a higher threshold altitude to define background values can also lead to higher uncertainties in air that is considered a background for local ABL measurements due to the fact that air at or above 4000 m a.m.s.l. may have experienced longer-range transport.

3 Results and discussion

3.1 Mid-Atlantic $\Delta^{14}\text{CO}_2$ background in general agreement with NOAA aircraft network

Figure 2a shows the vertical distribution of $\Delta^{14}\text{CO}_2$ measured for all seasonal campaigns between winter 2017 and summer 2019, highlighting this difference and indicating generally lower values and significantly greater variation relative to the FT throughout the bottommost troposphere due to surface emissions of ¹⁴C-free fossil fuels.

Figure 2b shows the decrease in atmospheric $\Delta^{14}\text{CO}_2$ in the FT over time during ACT and within the broader NOAA Global Greenhouse Gas Reference Network (GGGRN) due to global-scale addition of fossil fuel CO₂ and justifies the use of ACT FT for a definition of background atmospheric conditions. As expected, values of Δ_{bg} throughout the upper FT are relatively homogenous during each campaign and

are in rough agreement with other FT flask $\Delta^{14}\text{CO}_2$ measurements within the GGGRN (Sweeney et al., 2015; Miller et al., 2012) such as Cape May, NJ (CMA), and Portsmouth, NH (NHA). For fall and spring seasons, ACT FT $\Delta^{14}\text{CO}_2$ is slightly higher than that in the GGGRN sites, including the upwind high-altitude (3000–4000 m a.m.s.l.) Niwot Ridge, CO (NWR) site. During ACT, FT samples are frequently obtained from higher altitudes than the GGGRN $\Delta^{14}\text{CO}_2$ paired flask samples with fixed collection altitudes, resulting in the potential for ACT FT air to originate from different latitudes or altitudes where influence from cosmogenically produced ¹⁴CO₂ could explain deviations of $\sim 2\%$ above GGGRN $\Delta^{14}\text{CO}_2$ observations (Turnbull et al., 2009). Early in the ACT winter 2017 campaign, FT $\Delta^{14}\text{CO}_2$ is lower than the mean values in the GGGRN (Fig. 2b) and is accompanied by higher-than-average CO mole fractions. This result potentially indicates a small influence from local pollution sources that are depleted in FT $\Delta^{14}\text{CO}_2$. Nonetheless, these ACT FT data agree with ($\pm 1\sigma$ standard deviation) GGGRN continental background FT values and are included in this analysis.

Figure 3a highlights the spatial extent of flask sampling during the ACT mission and density of flask sampling over the four seasonal campaigns with an average $\Delta^{14}\text{CO}_2$ ABL minus FT difference of -5% . Using Eq. (4), CO_{2ff} is calculated for all flask samples, and general agreement between largely negative $\Delta^{14}\text{CO}_2$ ABL signals and higher CO_{2ff} signals is seen throughout ACT (Fig. 3b). ACT-observed CO_{2ff} ranges from -0.8 to 15.5 ppm, and we note that negative CO_{2ff} values are not physically realistic but can occur due to the measurement uncertainty of $\Delta^{14}\text{CO}_2$, by using an inappropriate $\Delta^{14}\text{CO}_2$ background value or by underestimating the CO_{2corr} term in Eq. (4). Compared to other surface and aircraft observations of CO_{2ff} throughout the USA, the range of ACT CO_{2ff} is comparable to CO_{2ff} measured in other studies in the Mid-Atlantic USA (Miller et al., 2012: -3 to 13 ppm CO_{2ff}), downwind of Sacramento, CA (Turnbull et al., 2011a: 2.4 – 8.6 ppm CO_{2ff}), and in the Colorado urban regions (Graven et al., 2009: 0 – 20 ppm CO_{2ff}). Maximum values of CO_{2ff} measured during ACT were, however, much lower than those over the densely populated urban area of Los Angeles, CA (Miller et al., 2020: -1.3 to 48.4 ppm CO_{2ff}), due to its more rural sampling focus. Few ACT flight legs were aimed at capturing local urban-scale CO_{2ff} signals. As such, the analysis below requires averaging of these signals as a more robust way to qualitatively analyze the ACT flask CO_{2ff} data.

3.2 Partitioning of seasonal CO_{2tot} indicates biogenic-driven variability

For consistency throughout ACT seasonal campaigns, ABL values for all species in the subsequent analysis are reported as an ABL minus FT difference. Figure 4 shows CO_{2ff} alongside biogenic CO₂ (CO_{2bio}) calculated from Eq. (1), dis-

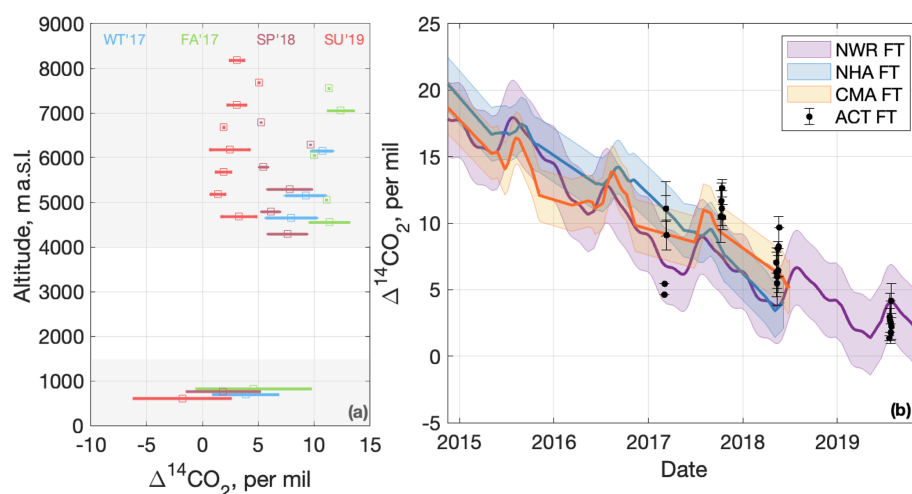


Figure 2. (a) Vertical distribution of $\Delta^{14}\text{CO}_2$ during all ACT campaigns in the Mid-Atlantic USA. ABL values shown are the average of all observations below 1500 m a.s.l. (values are separated vertically for clarity) for each seasonal campaign, while horizontal bars represent their 1σ standard deviation in time. FT values (altitudes greater than 4000 m a.s.l.) shown are 500 m binned averages and their 1σ standard deviation in $\Delta^{14}\text{CO}_2$ for each 500 m altitude bin. Shaded regions represent ABL and FT definitions. (b) Daily mean ACT FT $\Delta^{14}\text{CO}_2$ background measurements ($\pm 1\sigma$ standard deviation shading) are shown compared to NOAA GGGRN aircraft network $\Delta^{14}\text{CO}_2$ FT (~ 4000 m a.s.l.) measurements. GGGRN data are seasonal (3-month averaged) aircraft FT $\Delta^{14}\text{CO}_2$ obtained offshore of Cape May, NJ (CMA); offshore of Portsmouth, New Hampshire (NHA); and surface $\Delta^{14}\text{CO}_2$ for the high-altitude site Niwot Ridge, CO (NWR), at ~ 3500 m a.s.l.

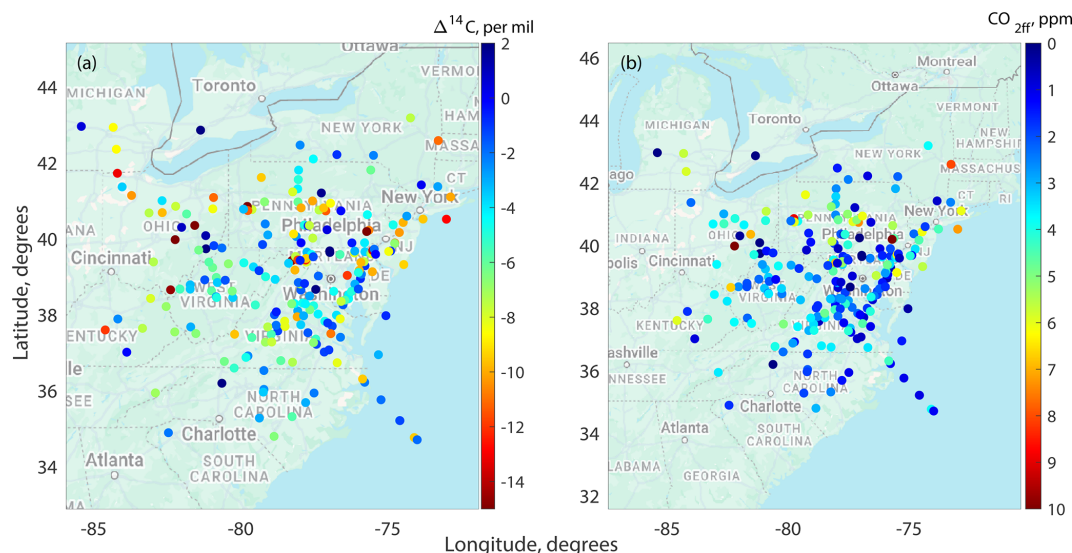


Figure 3. (a) $\Delta^{14}\text{CO}_2$ ABL minus FT differences for all seasons in the Mid-Atlantic USA. Note that the color bar is reversed to indicate warmer colors for more negative $\Delta^{14}\text{CO}_2$. (b) ABL CO_2ff calculated for the same flask samples shown in (a) for all seasons in the Mid-Atlantic USA. Plot maps are produced using Google Maps API (© Google Maps 2025).

played by month of the year for ACT deployments in winter (2017), spring (2018), summer (2019) and fall (2017) in the Mid-Atlantic United States. Total ($\text{CO}_{2\text{tot}}$), fossil fuel and biogenic CO_2 data are shown to indicate relative contributions to the observed $\text{CO}_{2\text{tot}}$ variability (Eq. 1). $\text{CO}_{2\text{tot}}$ observed in the ABL varies seasonally; while most often positive for flights conducted in late fall and winter, CO_2

depletion is seen during summer as expected due to net photosynthetic uptake by the terrestrial biosphere (Tans et al., 1990). Seasonal changes in ABL $\text{CO}_{2\text{tot}}$ were driven by $\text{CO}_{2\text{bio}}$, which varied from -19.7 ppm during summer flights to 16.2 ppm in late fall (Fig. 4). In early fall, negative $\text{CO}_{2\text{bio}}$ was observed (Fig. 4) from a strong surface influence and net uptake in southwestern Virginia (Fig. 1). For the remainder of

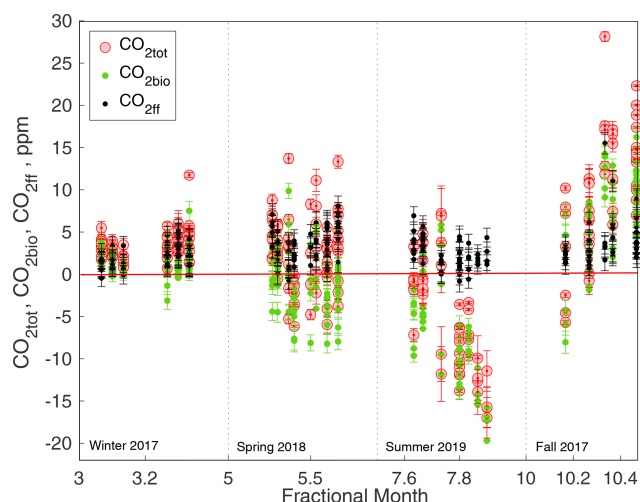


Figure 4. Calculated total CO₂ (CO_{2tot}), partitioned into biogenic CO₂ (CO_{2bio}) and fossil fuel CO₂ (CO_{2ff}) components using Eq. (4) in winter 2017, spring 2018, summer 2019, and fall 2017. As seasonal campaigns were not conducted consecutively within a single year, we examine variability according to a “climatological” year. Note that the x axis is intentionally non-linear to show intra-day variability. 1 σ error bars are shown for CO_{2tot}, CO_{2bio} and CO_{2ff}.

the fall campaign, flights indicated generally positive CO_{2bio} with net respiration and weaker surface influence. CO_{2ff} has a lower contribution to CO_{2tot} variability during ACT in the Mid-Atlantic region from one campaign to the next, with a positive contribution of 3.3 ± 2.0 ppm. Given the small number of flights shown over 3 years, it should be noted that the seasonality in CO_{2ff} may not represent true climatological CO_{2ff} variability and should not be interpreted in terms of uniform fossil fuel emissions, because there is likely seasonal variation in ABL depth, which can counteract seasonally varying emissions.

The flask sampling region for this study encompasses rural to suburban regions, reducing signal-to-noise ratio in $\Delta^{14}\text{CO}_2$ and complicating the interpretation of CO_{2tot} observed due to a wide mixture of surface sources (and sinks). As CO_{2tot} is largely controlled by CO_{2bio}, we correlate (using Pearson’s R^2 values) and regress CO_{2tot} with CO_{2ff} and with CO_{2bio} (see Table S1 in the Supplement). Regressions between CO_{2bio} and CO_{2tot} result in slopes between 0.86 and 0.92 for all seasons. Strong correlations between CO_{2bio} and CO_{2tot} exist from spring through to fall with R^2 values between 0.73 and 0.92. Somewhat strong relationships between CO_{2tot} and CO_{2bio} were found during the (March) winter 2017 campaign with a regression slope close to 1 but relatively weak correlation ($R^2 \sim 0.3$), which could partially be explained by small CO_{2ff} signals but also indicate that observed CO₂ had a non-negligible influence from biogenic CO₂ exchange as was also found in previous studies (Potosnak et al., 1999; Turnbull et al., 2006; Miller et al., 2012;

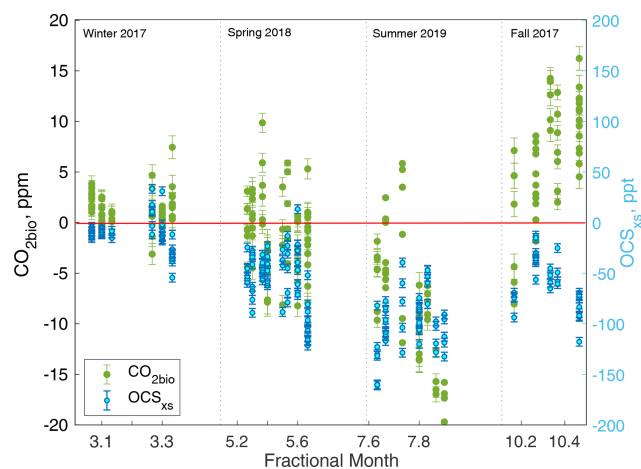


Figure 5. ABL biogenic CO₂ (CO_{2bio}) and OCS ABL minus FT difference (OCS_{xs}) in winter 2017; spring 2018; summer 2019; and fall 2017. As seasonal campaigns were not conducted consecutively within a single year, we examine variability according to a “climatological” year. Note that the x axis is intentionally non-linear to show intra-day variability. 1 σ error bars are shown for CO_{2bio} and OCS_{xs}.

Baier et al., 2020). Correlations between CO_{2tot} and CO_{2ff} are weak, with associated regression slopes highest during winter and smaller slopes observed for the spring, summer and fall deployments when ecosystem CO₂ fluxes are higher.

The fraction of negative CO_{2tot} during biogenically active months in spring (May), summer (July) and fall (October) are 28 %, 62 % and 4 %, respectively (Table S1). However, when examining the fraction of negative CO_{2bio} (indicating net CO₂ uptake), these percentages are much larger at 57 %, 82 % and 8 %, respectively. The difference between negative CO_{2tot} and negative CO_{2bio} fractions of 20 %–30 % during months when the ecosystems are more active highlights the importance of using $\Delta^{14}\text{CO}_2$ to enable partitioning of CO_{2tot} into fossil fuel and biogenic components; this would not be possible when considering CO_{2tot} alone, as a portion of this flux component would be masked by fossil fuel emissions.

We also examine carbonyl sulfide ABL minus FT differences (OCS_{xs}) alongside CO_{2bio} as an additional tracer for biogenic processing as OCS is taken up by plants similarly to CO₂ but not respired (Montzka et al., 2007; Campbell et al., 2008, Fig. 5). In Fig. 5, we observe a strong positive correlation with CO_{2bio} and OCS_{xs} when combining all seasonal ACT data except fall, where CO_{2bio} is either negative or weakly positive (see Fig. S1a in the Supplement), consistent with photosynthesis explaining negative CO_{2bio} values. A modest positive correlation ($R = 0.54$) is seen when also including fall ACT data. Including or excluding the winter data, given the insignificant slope between OCS_{xs} and CO_{2bio} (Table S1), does not affect this correlation.

For fall 2017, the overall correlation between CO_{2bio} and OCS_{xs} is low and not significant (Table S1). However, sta-

tistically significant correlations are seen between negative CO_{2bio} and OCS_{xs} in early fall due to continued uptake of CO₂ by the terrestrial biosphere (Fig. 5). A moderate negative correlation is observed between OCS_{xs} and CO_{2bio} in late fall after net respiration is seen to occur (Figs. 5 and S1b). During this time, CO_{2bio} values of up to ~ 16 ppm occur alongside relatively significant OCS_{xs} values of almost –120 ppt. The net negative correlation during fall between CO_{2bio} and OCS_{xs} indicates that while CO₂ uptake could still be occurring the magnitude of this process is not large enough to offset respiration. Similar to ACT, clear differences in the amplitude and phases of OCS and CO₂ cycles were first described in Montzka et al. (2007) and in other previous studies (Kuai et al., 2022; Ma et al., 2023). Furthermore, many OCS studies have found several instances where ecosystem OCS uptake is decoupled from gross primary productivity (GPP), including nighttime processes (Commane et al., 2015; Kooijmans et al., 2017; Hu et al., 2021), uptake from soil (Whelan et al., 2022) and/or senescing or decaying fall vegetation (Sun et al., 2016; Rastogi et al., 2018). Further studies could utilize colocated measurements such as OCS and radiocarbon-based CO_{2bio} to evaluate (a) the relationship between OCS and CO₂ cycles during the transition from net photosynthesis to net respiration and (b) regional model GPP and respiration fluxes. Further, we note that correlations between negative CO_{2tot} and OCS_{xs} weaken in the early fall due to proportionally high fossil fuel emissions, providing insufficient information about GPP. Parazoo et al. (2021) found that models underestimate observed CO_{2tot} during ACT and have decreased fidelity in reproducing GPP inferred from observations throughout the USA. Since stronger relationships emerge between OCS_{xs} and CO_{2bio} than OCS_{xs} and CO_{2tot}, again, using OCS and radiocarbon-based CO_{2bio} could further inform and constrain these model processes.

3.3 Example case: “pseudo-CO_{2ff}” as a product for evaluating model error

We use CO_{2ff} as a model “transport tracer” to examine model errors as CO_{2ff} fluxes are assumed to be relatively well-known (Turnbull et al., 2009). Well-known emissions and well-measured mole fractions directly tracing those emissions allow us to evaluate the atmospheric tracer transport that connects the two. Here, we compare a “pseudo-CO_{2ff}” or high-frequency CO_{2ff} (Eq. 5) to CO_{2ffmod} simulated using the PSUWRF forward model, based on averaged ODIAC and Miller fossil fuel emissions (Jacobson et al., 2020). This CO_{2ff} product, being high frequency, can also capture more diurnal variability in fossil fuel CO₂ and therefore evaluate modeled fossil fuel CO₂ more thoroughly than measurements made using discrete flask samples.

3.3.1 Variability and uncertainty of R_{CO} and CO_{2ff}

Our CO_{2ff} estimation relies on the assumption that the emission ratio of CO to CO_{2ff} (R_{CO}) is constant for a given flight day. As mentioned above, a median R_{CO} value for each day is used as opposed to a more general regression slope between flask CO ABL minus FT differences and CO_{2ff} because of low correlations between the two variables seasonally. We note that the numerator of R_{CO} represents the enhancement in all CO sources (fossil, but also potentially biomass burning and oxidation of volatile organic compounds – VOCs) as well as a very small amount of CO oxidative loss. Because all of these sources are “calibrated” relative to CO_{2ff} (the denominator), it is not necessary to explicitly define non-fossil components of this ratio.

Figure 6 indicates that the median R_{CO} calculated for all ACT missions ($10.03 \pm 8.15 \Delta\text{CO}$ per ppm CO_{2ff}; 68 % CI) is slightly higher than in urban studies (Turnbull et al., 2011a, 2015; Miller et al., 2012). Day-to-day or even diurnal R_{CO} is also largely variable, which could be a result of variability in CO_{2ff} or in measured background levels (which are represented by a single daily value). Spatial differences in VOC oxidation could play a minor role in influencing the variability of R_{CO} . CO additions from VOCs throughout the ACT Mid-Atlantic region will render R_{CO} higher. However, despite the expectation that greater oxidation of VOCs will produce more CO during the summer (Vimont et al., 2017), we see the highest average R_{CO} values during spring. R_{CO} variability in both the fall and spring campaigns suggest that there could be other influential mechanisms occurring, yet DiGangi et al. (2021) found that the biomass burning influences on air sampled during ACT were negligible in the Mid-Atlantic region, ruling out the possibility that biomass burning events contribute to the high variability of R_{CO} calculated here. In general, it is more likely that low CO_{2ff} signals with high relative uncertainties are creating abnormally high R_{CO} values using this median method in this work, which has also been found and discussed in great detail in Maier et al. (2024b).

As mentioned above, we calculate CO_{2ff} only for days when flask measurements were analyzed for $\Delta^{14}\text{CO}_2$. When comparing CO_{2ff} with flask-based CO_{2ff}, the mean bias is 0.7 ± 2.1 ppm (1σ) (Fig. 7). The relatively large standard deviation in Fig. 7 indicates that flask samples collected within a single research flight were not always representative of the entire domain surveyed on that day by continuous analyzers. Point sources of CO₂ from power plants that do not emit CO captured by continuous measurements could potentially skew this comparison alongside other non-fossil-fuel CO sources, but the small bias between the two suggests that CO_{2ff} is generally in good agreement with flask CO_{2ff}.

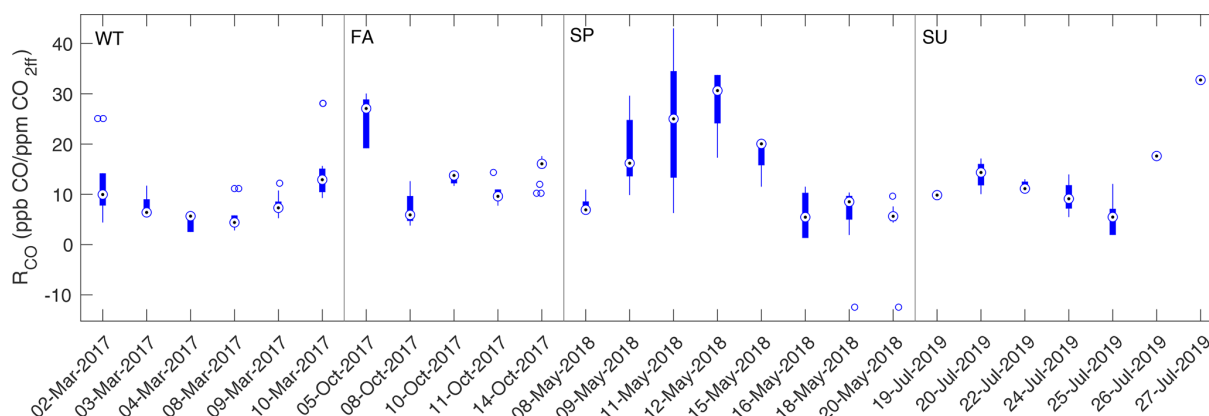


Figure 6. Daily R_{CO} calculated from discrete flask samples during winter (WT, 2017), fall (FA, 2017), spring (SP, 2018), and summer (SU, 2019). Note that, unlike Figs. 4 and 5, flight data are shown in chronological order. Median R_{CO} for each research flight is shown as a bullet point, with the interquartile (IQ) range shown as the thick bar line. Outliers greater than 1.5 times the IQ range are shown as separate open circles, and maximum extreme values as whiskers that do not qualify as outliers (thin lines), extending from the IQ ranges. Flask data shown are combined for B-200 and C-130 aircraft.

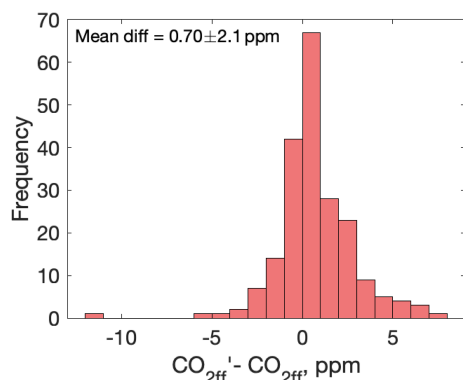


Figure 7. Histogram of in situ (CO'_{2ff}) minus flask-derived (CO_{2ff}) fossil fuel CO₂ for measurement times corresponding to the total campaign (winter 2017 through to summer 2019) in the Mid-Atlantic region. Here, CO'_{2ff} is calculated for corresponding flask sample times. By definition of CO_{2ff} and CO'_{2ff} above, this comparison indicates ABL sample comparisons only.

3.3.2 Comparison of CO'_{2ff} and CO_{2ffmod}

Figure 8 shows the average difference between CO_{2ffmod} computed along ACT flight tracks and ABL CO'_{2ff} . Several research flight days indicate rough agreement between CO_{2ffmod} and CO'_{2ff} within a mean of $\sim 0.49 \pm 2.6$ ppm (1σ) but higher differences outside of average CO'_{2ff} uncertainty bounds are seen in Fig. 8 along with a slight skewness. The mapped extent of this positive bias in CO_{2ffmod} is visualized in Fig. 9 for fall 2017, spring 2018 and summer 2019 campaigns, while the winter 2017 campaign model bias in CO_{2ffmod} is slightly negative.

While there are logistical advantages to using this “pseudo- CO_{2ff} ” method from a $\Delta^{14}CO_2$ measurement capacity standpoint, this product has a higher average un-

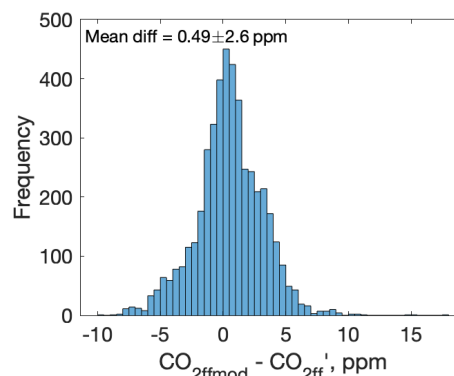


Figure 8. Histogram of PSUWRF $CO_{2ffmod} - CO'_{2ff}$ for all flask $\Delta^{14}CO_2$ sample days between winter 2017 and summer 2019 in the Mid-Atlantic region.

certainty (4.96 ppm) associated with large intra-day background variability and assumptions in the value of R_{CO} . For this reason, we caution the overgeneralization of the use of CO_{2ff} as a transport tracer with this dataset and have chosen 24 July 2019 as an example of when positively biased CO_{2ffmod} can be evaluated using CO'_{2ff} . Here, a series of B-200 flights was conducted downwind of three major eastern US cities (New York City, NY; Philadelphia, PA; and Washington, D.C.). ABL flask sampling on each flight leg informed the derivation of CO'_{2ff} , and both estimates are in rough agreement as seen in Fig. 10. This individual flight day had higher fossil fuel CO₂ signals and lower variability in background CO measurements, with a lower CO'_{2ff} uncertainty (~ 2 ppm) relative to the campaign-wide average.

Figure 11 shows calculated CO'_{2ff} along three ABL flight legs with large positive fossil fuel CO₂ downwind of these urban areas. Comparing modeled (CO_{2ffmod}), calcu-

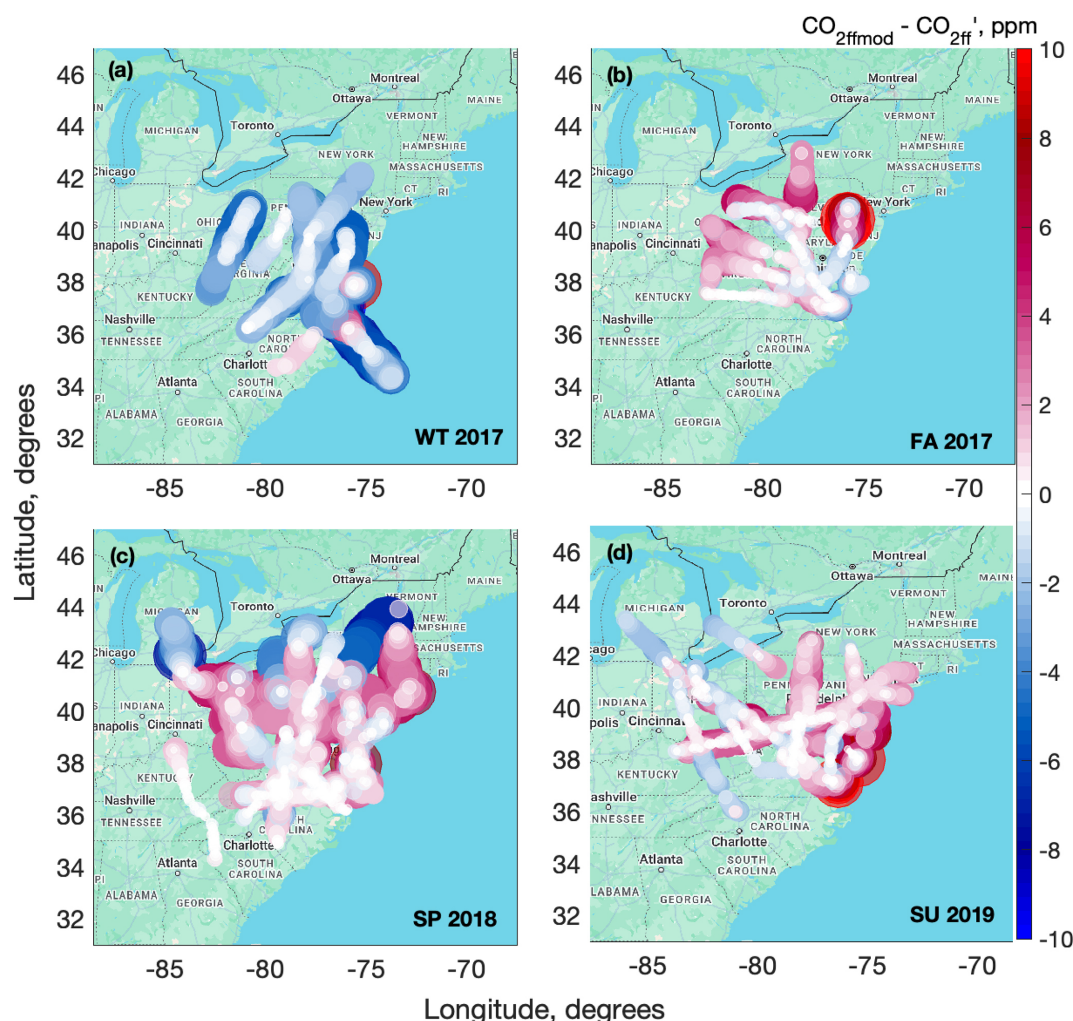


Figure 9. Mapped modeled versus $\text{CO}'_{2\text{ff}}$ for flask $\Delta^{14}\text{CO}_2$ sample flight days for (a) winter (WT) 2017, (b) fall (FA) 2017, (c) spring (SP) 2018 and (d) summer (SU) 2019 campaigns. Points are sized by the model minus data differences. Plot maps are produced using Google Maps API (© Google Maps 2025).

lated ($\text{CO}'_{2\text{ff}}$) and flask-derived ($\text{CO}_{2\text{ff}}$) $\text{CO}_{2\text{ff}}$, we find that $\text{CO}'_{2\text{ff}}$ plumes observed downwind of cities do not always align with $\text{CO}_{2\text{ffmod}}$ throughout the research flight. Significant differences are observed between $\text{CO}_{2\text{ffmod}}$ and $\text{CO}'_{2\text{ff}}$ magnitudes, particularly during the Washington, D.C., flight leg of up to 60 % beyond uncertainty bounds, with the urban emissions plume misaligned (Fig. 11). $\text{CO}_{2\text{ffmod}}$ is consistently higher than $\text{CO}'_{2\text{ff}}$ in the Philadelphia flight leg as well, with general agreement in the plume variability. Finally, we note that the PSUWRF model simulates $\text{CO}_{2\text{ff}}$ in the New York City flight leg relatively well with respect to flask $\text{CO}_{2\text{ff}}$.

Current uncertainties of CO_2 fossil fuel fluxes, based on differences among various emissions products, are less than or equal to 20 % at the regional scale (Gurney et al., 2020), and this is corroborated in the PSUWRF model, where Feng et al. (2019a) note that the uncertainty in fossil fuel fluxes on a daily average timescale is approximately 20 %. This un-

certainty may increase at the hourly timescale and certainly within smaller urban-scale domains (Gately and Hutrya, 2017). We investigate several reasons for the 60 % overestimation in simulated $\text{CO}_{2\text{ff}}$ beyond the larger calculated $\text{CO}'_{2\text{ff}}$ uncertainty bounds and the misalignment of the Washington, D.C., $\text{CO}_{2\text{ffmod}}$ “plume” relative to $\text{CO}'_{2\text{ff}}$. First, this discrepancy cannot be explained by model deviations in key meteorological variables such as wind speed, wind direction or ABL depth relative to observations. The PSUWRF modeled wind speeds and directions compare well to in situ wind speed and directions along the B-200 flight track to within 1 m s^{-1} and 10° , respectively. ABL depths derived from B-200 potential temperature soundings flown at the endpoints of each urban transect in Fig. 11 also compare well with ABL depth, estimated from PSUWRF potential temperature to within 300 m on average. Second, emissions uncertainties within PSUWRF could result in observed differences be-

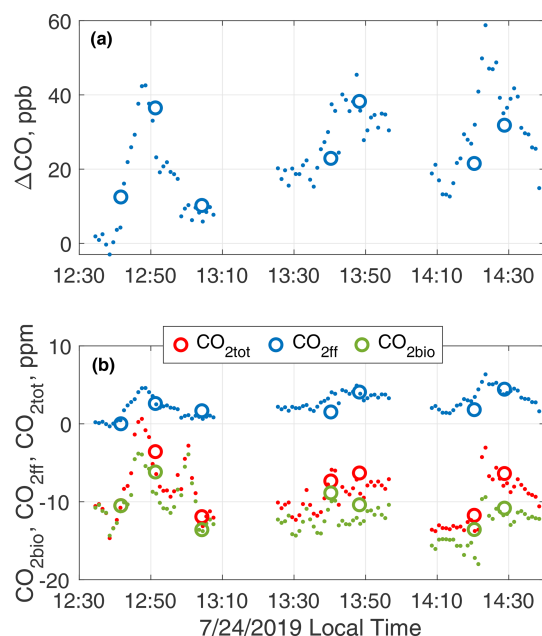


Figure 10. In situ (points) and flask (circles) observations for the B-200 aircraft on 24 July 2019. **(a)** CO ABL minus FT differences (ΔCO) calculated from flasks and in situ continuous measurements. ΔCO from flasks is used to calculate R_{CO} and thus $\text{CO}'_{2\text{ff}}$ using Eq. (5) using in situ measurements. The average difference in ΔCO (in situ minus flask) is 0.6 ± 8.7 ppb. **(b)** $\text{CO}_{2\text{bio}}$, $\text{CO}'_{2\text{ff}}$ and $\text{CO}_{2\text{tot}}$ calculated from both in situ high-frequency data (points) and from flask measurements (circles) on 24 July 2019 show good agreement. Average differences in $\text{CO}_{2\text{bio}}$, $\text{CO}'_{2\text{ff}}$ and $\text{CO}_{2\text{tot}}$ (in situ minus flask) are -1.6 ± 1.2 , 1.2 ± 1.3 and 0.4 ± 1.2 ppm, respectively.

tween $\text{CO}'_{2\text{ff}}$ and $\text{CO}_{2\text{ffmod}}$ of this magnitude. One hypothesis is that if multiple fossil fuel emissions datasets are run independently in PSUWRF and the ensemble of these simulations is narrow, then more confidence can be gained in that the differences in Fig. 11 are not due to errors in fluxes but rather errors in model transport. PSUWRF simulations between 2017–2018 indicate that independently run fossil fuel emissions fields with differing spatial and temporal resolutions (i.e., ODIAC and Miller fields) result in small $\text{CO}_{2\text{ffmod}}$ differences that are within 1.5–2 ppm on average. While these fossil fuel emissions products were not run separately in the PSUWRF model beyond 2018, a 2 ppm $\text{CO}_{2\text{ffmod}}$ variability is substantially smaller than that shown in Fig. 11 downwind of Washington and Philadelphia (3–6 ppm $\text{CO}_{2\text{ff}}$). It is possible that the model vertical transport parameterizations are erroneous earlier in the day, which could produce errors later in the day in $\text{CO}_{2\text{ff}}$ accumulation and venting relative to that observed downwind of Washington, D.C., and even Philadelphia, PA. Therefore, while our current results suggest that model transport rather than fluxes are erroneous on this particular flight, the results from this case study are important to document for future model–observation com-

parisons. More intensive work beyond the scope of this work would be needed to verify our hypothesis, which could involve model runs with a number of both transport and flux variants to discern model variability with different realistic ensemble members. Within this type of study, observed and modeled values for additional urban campaign data should also be compared.

While this example does not represent the average $\text{CO}_{2\text{ffmod}}$ bias with respect to $\text{CO}'_{2\text{ff}}$ during ACT, it illustrates the utility of $\text{CO}'_{2\text{ff}}$ as a model transport tracer. In the above example, the high-frequency $\text{CO}'_{2\text{ff}}$ product is able to easily highlight potential modeled errors in the representation of diurnal $\text{CO}_{2\text{ff}}$ plume variability. As discussed in Miller et al. (2020), deriving $\text{CO}'_{2\text{ff}}$ in this way, using information gleaned from a small subset of $\Delta^{14}\text{CO}_2$ flask sample measurements, can provide a means for determining the fossil fuel and biogenic components of $\text{CO}_{2\text{tot}}$ for regional or city-scale studies. Despite higher average uncertainties than flask-based methods, comparisons to models might allow for examination and improvements upon gross model errors for more accurate CO₂ mole fraction estimation and process-based studies. As mentioned above, differentiating between regional model transport and flux errors might be improved upon in the future by using an ensemble of both transport and flux variants. As ACT $\Delta^{14}\text{CO}_2$ flask sampling was generally aimed at capturing broad-scale biogenic CO₂ features across the eastern USA, more targeted flask sampling in urban areas with larger $\text{CO}_{2\text{ff}}$ signals could reduce R_{CO} and $\text{CO}'_{2\text{ff}}$ uncertainties, which would allow for more robust $\Delta^{14}\text{CO}_2$ -based model verification using comparatively fewer flask samples. At more rural sites, a greater number of flask samples may be needed to robustly calculate $\text{CO}'_{2\text{ff}}$ (Maier et al., 2024b).

4 Conclusions

The ACT-America mission, while focused on improving the accuracy of regional carbon flux estimates, also provided the opportunity for a dense seasonally diverse dataset of atmospheric $\Delta^{14}\text{CO}_2$ measurements from flasks sampled throughout the Mid-Atlantic USA and the capability to disaggregate total CO₂ into biogenic and fossil fuel components, which is critical for regional CO₂ source attribution. Seasonal campaigns occurring between 2017 and 2019 indicated that biogenic CO₂ exchange in the Mid-Atlantic was the primary driver of CO₂ boundary layer variability in this region as expected, while $\text{CO}_{2\text{ff}}$ remained relatively constant during the ACT mission. Consistent OCS uptake in all seasons was observed that correlated well with negative $\text{CO}_{2\text{bio}}$, confirming CO₂ uptake by photosynthesis throughout the ACT campaigns, though instances were seen where OCS uptake was clearly decoupled from gross primary productivity during the fall. With the broad nature of flask sampling during ACT, the signal-to-noise (measurement precision) ratio in $\Delta^{14}\text{CO}_2$ data was low, and campaigns investigating strictly

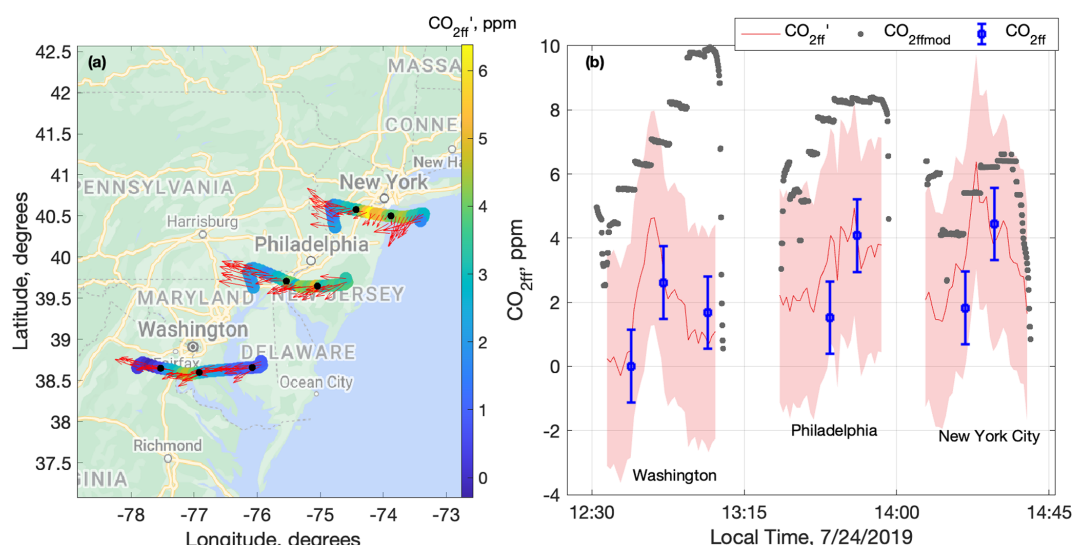


Figure 11. (a) Pseudo- $\text{CO}_{2\text{ff}}$ ($\text{CO}'_{2\text{ff}}$) calculated along the ACT B-200 ABL flight track on 24 July 2019 (plot produced using Google Maps API, © Google Maps 2025). Flight tracks are colored by $\text{CO}'_{2\text{ff}}$ which proceed northerly from Washington, D.C., to New York City, NY. Black points indicate flask sample locations. Red arrows indicate the wind direction as calculated from aircraft flight data. (b) Fossil fuel CO_2 calculated from in situ measurements ($\text{CO}'_{2\text{ff}}$), from flask $\Delta^{14}\text{CO}_2$ ($\text{CO}_{2\text{ff}}$) and from PSUWRF using CT fossil fuel emissions ($\text{CO}_{2\text{ffmod}}$). Discretization in $\text{CO}_{2\text{ffmod}}$ is due to the native 27 km resolution of PSUWRF. Error shading for $\text{CO}'_{2\text{ff}}$ is the derived 1σ uncertainty in the $\text{CO}'_{2\text{ff}}$ calculation for 24 July 2019 and error bars for flask $\text{CO}_{2\text{ff}}$ reflect a 1σ uncertainty.

urban CO_2 signals can better highlight the utility that routine observations of $\Delta^{14}\text{CO}_2$ can provide, including critical information for stakeholders in assessing carbon reduction strategies on regional to sub-regional scales. Several studies have shown the value of incorporating $\Delta^{14}\text{CO}_2$ alongside CO_2 measurements as an improved model constraint on regional CO_2 fluxes, and future work will require a continued effort to ensure routine $\Delta^{14}\text{CO}_2$ measurements throughout the NOAA GGGRN and other networks. Here, we have used flask $\Delta^{14}\text{CO}_2$ samples, taken alongside continuous in situ CO measurements, to provide a high-frequency “pseudo- $\text{CO}_{2\text{ff}}$ ” product ($\text{CO}'_{2\text{ff}}$) using the relationship between in situ CO ABL minus FT differences and flask-derived $\text{CO}_{2\text{ff}}$. This product was used to evaluate modeled $\text{CO}_{2\text{ff}}$ at a higher temporal resolution than discrete flasks can provide and to illuminate potential errors in model transport at the regional scale. Although the ACT dataset and analysis therein are limited by higher $\text{CO}'_{2\text{ff}}$ uncertainties, as well as limited to days when $\Delta^{14}\text{CO}_2$ signals are higher, this work highlights the value of such a product in future campaigns and measurement networks as a model evaluation tool.

Data availability. Observational in situ and flask data from the NASA ACT-America mission used for the analysis in this study are publicly archived at the Oak Ridge National Laboratory repository at <https://doi.org/10.3334/ORNLDAAAC/1593> (Davis et al., 2018) in addition to PSUWRF output for the ACT-America campaign at <https://doi.org/10.3334/ORNLDAAAC/1884> (Feng et al., 2021b). Individual flask data with $^{14}\text{CO}_2$ measurements from ACT-America

can be found at (<https://doi.org/10.3334/ORNLDAAAC/1575>, Sweeney et al., 2018). All data are synced to meteorological and location data aboard each aircraft and available for downloading and merging (<https://doi.org/10.3334/ORNLDAAAC/1574>, Yang et al., 2018). GGGRN $\Delta^{14}\text{CO}_2$ and CO flask data used to supplement this study from NWR, NHA and CMA are available at <https://doi.org/10.15138/87ny-6277> (Baier et al., 2024). The NOAA HYSPLIT model is publicly available via <https://www.ready.noaa.gov/HYSPLIT.php> (last access: 13 February 2024) for registered and unregistered versions.

Supplement. The supplement related to this article is available online at <https://doi.org/10.5194/acp-25-10479-2025-supplement>.

Author contributions. BCB led the investigation and curated the data alongside JPD, YC, SL and CW. CS, KD, JM, JPD and SL assisted with acquiring funding for this work. BB, JM and SL conceptualized the analysis and contributed to writing the original draft of this paper. SF and TL developed and contributed model analysis and output. All authors contributed to reviewing and editing the manuscript.

Competing interests. The contact author has declared that none of the authors has any competing interests.

Disclaimer. Publisher’s note: Copernicus Publications remains neutral with regard to jurisdictional claims made in the text, pub-

lished maps, institutional affiliations, or any other geographical representation in this paper. While Copernicus Publications makes every effort to include appropriate place names, the final responsibility lies with the authors.

Acknowledgements. The authors thank two reviewers, Fabian Maier and Jocelyn Turnbull, who provided insightful comments and suggestions to improve this paper. We acknowledge the collaboration between NOAA Global Monitoring Laboratory (GML) and its cooperative partners, including its collaboration with the Cooperative Institute for Research in Environmental Sciences (CIRES) and facilities available to the Institute for Arctic and Alpine Research (INSTAAR). The authors thank Jocelyn Turnbull and Stephen Montzka for early, helpful discussions of data analysis methods and to Zachary Barkley for conducting PSUWRF model–observation comparisons of meteorological variables. We also acknowledge the critical work of NOAA/GML personnel Patricia Lang, Andrew Crotwell, Monica Madronich, Eric Moglia, Benjamin R. Miller, Duane Kitzis and Molly Crotwell with the measurement of flask samples and calibration of measurements, as well as NOAA collaborative partners throughout the GGGRN with the collection of aircraft flask samples at CMA, NHA and NWR. We acknowledge that this work would not have been made possible without significant help from the ACT-America science team, pilots and NASA management support.

Financial support. This research has been supported by the National Aeronautics and Space Administration (grant nos. NNX15AJ06G and NNX15AG76G), the Cooperative Institute for Research in Environmental Sciences (grant no. NA17OAR4320101), and the National Aeronautics and Space Administration (grant no. 80HQTR21T0069). The Pacific Northwest National Laboratory is operated by Battelle Memorial Institute under contract DE-AO5-76RL0 1830.

Review statement. This paper was edited by Tanja Schuck and reviewed by Fabian Maier and Jocelyn Turnbull.

References

- Andres, R. J., Boden, T. A., Breon, F.-M., Ciais, P., Davis, S., Erickson, D., Gregg, J. S., Jacobson, A., Marland, G., Miller, J., Oda, T., Oliver, J. G. J., Raupach, M. R., Rayner, P., and Treanton, K.: A synthesis of carbon dioxide emissions from fossil-fuel combustion, *J. Biogeosciences*, 9, 1845–1871, <https://doi.org/10.5194/bg-9-1845-2012>, 2012.
- Baier, B. C., Sweeney, C., Choi, Y., Davis, K. J., DiGangi, J. P., Feng, S., Fried, A., Halliday, H., Higgs, J., Lauvaux, T., Miller, B. R., Montzka, S. A., Newberger, T., Nowak, J. B., Patra, P., Richter, D., Walega, J., and Weibring, P.: Multi-species Assessment of Factors Influencing Regional CO₂ and CH₄ Enhancements During the Winter 2017 ACT-America Campaign, *J. Geophys. Res.-Atmos.*, 125, e2019JD031339, <https://doi.org/10.1029/2019JD031339>, 2020.
- Baier, B., Lehman, S., Miller, J., Wolak, C., and NOAA Global Monitoring Laboratory: Data in support of “Mid-Atlantic U.S. observations of radiocarbon in CO₂: biogenic and fossil source partitioning and model comparisons”, Version 20241105, NOAA GML [Data set], <https://doi.org/10.15138/87NY-6277>, 2024.
- Ballantyne, A. P., Alden, C. B., Miller, J. B., Tans, P. P., and White, J. W. C.: Increase in observed net carbon dioxide uptake by land and oceans during the past 50 years, *Nature*, 488, 70–72, <https://doi.org/10.1038/nature11299>, 2012.
- Basu, S., Miller, J. B., and Lehman, S.: Separation of biospheric and fossil fuel fluxes of CO₂ by atmospheric inversion of CO₂ and ¹⁴CO₂ measurements: Observation System Simulations, *Atmos. Chem. Phys.*, 16, 5665–5683, <https://doi.org/10.5194/acp-16-5665-2016>, 2016.
- Basu, S., Lehman, S. J., Miller, J. B., Andrews, A. E., Sweeney, C., Gurney, K. R., Xu, X., Southon, J., and Tans, P. P.: Estimating US fossil fuel CO₂ emissions from measurements of ¹⁴C in atmospheric CO₂, *P. Natl. Acad. Sci. USA*, 117, 13300–13307, <https://doi.org/10.1073/pnas.1919032117>, 2020.
- Brophy, K., Graven, H., Manning, A. J., White, E., Arnold, T., Fischer, M. L., Jeong, S., Cui, X., and Rigby, M.: Characterizing uncertainties in atmospheric inversions of fossil fuel CO₂ emissions in California, *Atmos. Chem. Phys.*, 19, 2991–3006, <https://doi.org/10.5194/acp-19-2991-2019>, 2019.
- Campbell, J. E., Carmichael, G. R., Chai, T., Mena-Carrasco, M., Tang, Y., Blake, D. R., Blake, N. J., Vay, S. A., Collatz, G. J., Baker, I., Berry, J. A., Montzka, S. A., Sweeney, C., Schnoor, J. L., and Stanier, C. O.: Photosynthetic Control of Atmospheric Carbonyl Sulfide During the Growing Season, *Science*, 322, 1085–1088, <https://doi.org/10.1126/science.1164015>, 2008.
- Ciais, P., Rayner, P., Chevallier, F., Bousquet, P., Logan, M., Peylin, P., and Ramonet, M.: Atmospheric inversions for estimating CO₂ fluxes: methods and perspectives, *Climatic Change*, 103, 69–92, <https://doi.org/10.1007/s10584-010-9909-3>, 2010.
- Commane, R., Meredith, L. K., Baker, I. T., Berry, J. A., Munger, J. W., Montzka, S. A., Templer, P. H., Juice, S. M., Zahniser, M. S., and Wofsy, S. C.: Seasonal fluxes of carbonyl sulfide in a midlatitude forest, *P. Natl. Acad. Sci. USA*, 112, 14162–14167, <https://doi.org/10.1073/pnas.1504131112>, 2015.
- Davis, K. J., Obland, M. D., Lin, B., Lauvaux, T., O’dell, C., Meadows, B., Browell, E. V., Digangi, J. P., Sweeney, C., McGill, M. J., Barrick, J. D., Nehrir, A. R., Yang, M. M., Bennett, J. R., Baier, B. C., Roiger, A., Pal, S., Gerken, T., Fried, A., Feng, S., Shrestha, R., Shook, M. A., Chen, G., Campbell, L. J., Barkley, Z. R., and Pauly, R. M.: ACT-America: L3 Merged In Situ Atmospheric Trace Gases and Flask Data, Eastern USA, ORNL DAAC [data set], <https://doi.org/10.3334/ORNLDAAC/1593>, 2018.
- Davis, K. J., Browell, E. V., Feng, S., Lauvaux, T., Obland, M. D., Pal, S., Baier, B. C., Baker, D. F., Baker, I. T., Barkley, Z. R., Bowman, K. W., Cui, Y. Y., Denning, A. S., DiGangi, J. P., Dobler, J. T., Fried, A., Gerken, T., Keller, K., Lin, B., Nehrir, A. R., Normile, C. P., O’Dell, C. W., Ott, L. E., Roiger, A., Schuh, A. E., Sweeney, C., Wei, Y., Weir, B., Xue, M., and Williams, C. A.: The Atmospheric Carbon and Transport (ACT)-America Mission, *B. A. Meteorol. Soc.*, 102, E1714–E1734, <https://doi.org/10.1175/BAMS-D-20-0300.1>, 2021.
- DiGangi, J. P., Choi, Y., Nowak, J. B., Halliday, H. S., Diskin, G. S., Feng, S., Barkley, Z. R., Lauvaux, T., Pal, S., Davis, K. J., Baier, B. C., and Sweeney, C.: Seasonal Variabil-

- ity in Local Carbon Dioxide Biomass Burning Sources Over Central and Eastern US Using Airborne In Situ Enhancement Ratios, *J. Geophys. Res.-Atmos.*, 126, e2020JD034525, <https://doi.org/10.1029/2020JD034525>, 2021.
- Feng, S., Lauvaux, T., Keller, K., Davis, K. J., Rayner, P., Oda, T., and Gurney, K. R.: A Road Map for Improving the Treatment of Uncertainties in High-Resolution Regional Carbon Flux Inverse Estimates, *Geophys. Res. Lett.*, 46, 13461–13469, <https://doi.org/10.1029/2019GL082987>, 2019a.
- Feng, S., Lauvaux, T., Davis, K. J., Keller, K., Zhou, Y., Williams, C., Schuh, A. E., Liu, J., and Baker, I.: Seasonal Characteristics of Model Uncertainties From Biogenic Fluxes, Transport, and Large-Scale Boundary Inflow in Atmospheric CO₂ Simulations Over North America, *J. Geophys. Res.-Atmos.*, 124, 14325–14346, <https://doi.org/10.1029/2019JD031165>, 2019b.
- Feng, S., Lauvaux, T., Williams, C. A., Davis, K. J., Zhou, Y., Baker, I., Barkley, Z. R., and Wesloh, D.: Joint CO₂ Mole Fraction and Flux Analysis Confirms Missing Processes in CASA Terrestrial Carbon Uptake Over North America, *Global Biogeochem. Cy.*, 35, e2020GB006914, <https://doi.org/10.1029/2020GB006914>, 2021a.
- Feng, S., Lauvaux, T., Barkley, Z. R., Davis, K. J., Butler, M. P., Deng, A., Gaudet, B., and Stauffer, D.: ACT-America: WRF-Chem Baseline Simulations for North America, 2016–2019, ORNL DAAC [data set], <https://doi.org/10.3334/ORNLDAAC/1884>, 2021b.
- Fischer, M. L., Parazoo, N., Brophy, K., Cui, X., Jeong, S., Liu, J., Keeling, R., Taylor, T. E., Gurney, K., Oda, T., and Graven, H.: Simulating estimation of California fossil fuel and biosphere carbon dioxide exchanges combining in situ tower and satellite column observations, *J. Geophys. Res.-Atmos.*, 122, 3653–3671, <https://doi.org/10.1002/2016JD025617>, 2017.
- Friedlingstein, P., O'Sullivan, M., Jones, M. W., Andrew, R. M., Gregor, L., Hauck, J., Le Quéré, C., Luijkx, I. T., Olsen, A., Peters, G. P., Peters, W., Pongratz, J., Schwingshackl, C., Sitch, S., Canadell, J. G., Ciais, P., Jackson, R. B., Alin, S. R., Alkama, R., Arneth, A., Arora, V. K., Bates, N. R., Becker, M., Belouin, N., Bittig, H. C., Bopp, L., Chevallier, F., Chini, L. P., Cronin, M., Evans, W., Falk, S., Feely, R. A., Gasser, T., Gehlen, M., Gkritzalis, T., Gloege, L., Grassi, G., Gruber, N., Gürses, Ö., Harris, I., Hefner, M., Houghton, R. A., Hurtt, G. C., Iida, Y., Ilyina, T., Jain, A. K., Jersild, A., Kadono, K., Kato, E., Kennedy, D., Klein Goldewijk, K., Knauer, J., Korsbakken, J. I., Landschützer, P., Lefèvre, N., Lindsay, K., Liu, J., Liu, Z., Marland, G., Mayot, N., McGrath, M. J., Metzl, N., Monacchi, N. M., Munro, D. R., Nakaoka, S.-I., Niwa, Y., O'Brien, K., Ono, T., Palmer, P. I., Pan, N., Pierrot, D., Pockock, K., Poulter, B., Resplandy, L., Robertson, E., Rödenbeck, C., Rodriguez, C., Rosan, T. M., Schwinger, J., Séférian, R., Shutler, J. D., Skjelvan, I., Steinhoff, T., Sun, Q., Sutton, A. J., Sweeney, C., Takao, S., Tanhua, T., Tans, P. P., Tian, X., Tian, H., Tilbrook, B., Tsjino, H., Tubiello, F., van der Werf, G. R., Walker, A. P., Wankinkhof, R., Whitehead, C., Willstrand Wranne, A., Wright, R., Yuan, W., Yue, C., Yue, X., Zaehle, S., Zeng, J., and Zheng, B.: Global Carbon Budget 2022, *Earth Syst. Sci. Data*, 14, 4811–4900, <https://doi.org/10.5194/essd-14-4811-2022>, 2022.
- Gately, C. K. and Hutry, L. R.: Large Uncertainties in Urban-Scale Carbon Emissions, *J. Geophys. Res.-Atmos.*, 122, 11242–11260, <https://doi.org/10.1002/2017JD027359>, 2017.
- Gerken, T., Feng, S., Keller, K., Lauvaux, T., DiGangi, J. P., Choi, Y., Baier, B., and Davis, K. J.: Examining CO₂ Model Observation Residuals Using ACT-America Data, *J. Geophys. Res.-Atmospheres*, 126, e2020JD034481, <https://doi.org/10.1029/2020JD034481>, 2021.
- Godwin, H.: Radiocarbon Dating: Fifth International Conference, *Nature*, 195, 943–945, <https://doi.org/10.1038/195943a0>, 1962.
- Graven, H., Keeling, R. F., and Rogelj, J.: Changes to Carbon Isotopes in Atmospheric CO₂ Over the Industrial Era and Into the Future, *Global Biogeochem. Cy.*, 34, e2019GB006170, <https://doi.org/10.1029/2019GB006170>, 2020.
- Graven, H. D. and Gruber, N.: Continental-scale enrichment of atmospheric ¹⁴C from the nuclear power industry: potential impact on the estimation of fossil fuel-derived CO₂, *Atmos. Chem. Phys.*, 11, 12339–12349, <https://doi.org/10.5194/acp-11-12339-2011>, 2011.
- Graven, H. D., Stephens, B. B., Guilderson, T. P., Campos, T. L., Schimel, D. S., Campbell, J. E., and Keeling, R. F.: Vertical profiles of biospheric and fossil fuel-derived CO₂ and fossil fuel CO₂:CO ratios from airborne measurements of $\Delta^{14}\text{C}$, CO₂ and CO above Colorado, USA, *Tellus B*, 61, 536–546, <https://doi.org/10.1111/j.1600-0889.2009.00421.x>, 2009.
- Gregg, J. S., Losey, L. M., Andres, R. J., Blasing, T. J., and Marland, G.: The Temporal and Spatial Distribution of Carbon Dioxide Emissions from Fossil-Fuel Use in North America, *J. Appl. Meteorol. Clim.*, 48, 2528–2542, <https://doi.org/10.1175/2009JAMC2115.1>, 2009.
- Gurney, K. R., Law, R. M., Denning, A. S., Rayner, P. J., Baker, D., Bousquet, P., Bruhwiler, L., Chen, Y.-H., Ciais, P., Fan, S., Fung, I. Y., Gloor, M., Heimann, M., Higuchi, K., John, J., Kowalczyk, E., Maki, T., Maksyutov, S., Peylin, P., Prather, M., Pak, B. C., Sarmiento, J., Taguchi, S., Takahashi, T., and Yuen, C.-W.: TransCom 3 CO₂ inversion intercomparison: 1. Annual mean control results and sensitivity to transport and prior flux information, *Tellus B*, 55, 555–579, <https://doi.org/10.1034/j.1600-0889.2003.00049.x>, 2003.
- Gurney, K. R., Liang, J., Patarasuk, R., Song, Y., Huang, J., and Roest, G.: The Vulcan Version 3.0 High-Resolution Fossil Fuel CO₂ Emissions for the United States, *J. Geophys. Res.-Atmos.*, 125, e2020JD032974, <https://doi.org/10.1029/2020JD032974>, 2020.
- Gurney, K. R., Liang, J., Roest, G., Song, Y., Mueller, K., and Lauvaux, T.: Under-reporting of greenhouse gas emissions in U.S. cities, *Nat. Commun.*, 12, 553, <https://doi.org/10.1038/s41467-020-20871-0>, 2021.
- Hayes, D. J., Turner, D. P., Stinson, G., McGuire, A. D., Wei, Y., West, T. O., Heath, L. S., de Jong, B., McConkey, B. G., Birdsey, R. A., Kurz, W. A., Jacobson, A. R., Huntzinger, D. N., Pan, Y., Post, W. M., and Cook, R. B.: Reconciling estimates of the contemporary North American carbon balance among terrestrial biosphere models, atmospheric inversions, and a new approach for estimating net ecosystem exchange from inventory-based data, *Global Change Biol.*, 18, 1282–1299, <https://doi.org/10.1111/j.1365-2486.2011.02627.x>, 2012.
- Hu, L., Montzka, S. A., Kaushik, A., Andrews, A. E., Sweeney, C., Miller, J., Baker, I. T., Denning, S., Campbell, E., Shiga, Y. P., Tans, P., Siso, M. C., Crotwell, M., McKain, K., Thoning, K., Hall, B., Vimont, I., Elkins, J. W., Whelan, M. E., and Suntharalingam, P.: COS-derived GPP relationships with temperature

- and light help explain high-latitude atmospheric CO₂ seasonal cycle amplification, *P. Natl. Acad. Sci. USA*, 118, e2103423118, <https://doi.org/10.1073/pnas.2103423118>, 2021.
- Jacobson, A. R., Schuldt, K. N., Miller, J. B., Oda, T., Tans, P., Arlyn Andrews, Mund, J., Ott, L., Collatz, G. J., Aalto, T., Afshar, S., Aikin, K., Aoki, S., Apadula, F., Baier, B., Bergamaschi, P., Beyersdorf, A., Biraud, S. C., Bollenbacher, A., Bowling, D., Brailsford, G., Abshire, J. B., Chen, G., Chen, H., Chmura, L., Climadat, S., Colomb, A., Conil, S., Cox, A., Cristofanelli, P., Cuevas, E., Curcoll, R., Sloop, C. D., Davis, K., Wekker, S. D., Delmotte, M., DiGangi, J. P., Dlugokencky, E., Ehleringer, J., Elkins, J. W., Emmenegger, L., Fischer, M. L., Forster, G., Frumau, A., Galkowski, M., Gatti, L. V., Gloor, E., Griffis, T., Hammer, S., Haszpra, L., Hatakka, J., Heliasz, M., Hensen, A., Hermanssen, O., Hintsa, E., Holst, J., Jaffe, D., Karion, A., Kawa, S. R., Keeling, R., Keronen, P., Kolari, P., Kominkova, K., Kort, E., Krummel, P., Kubistin, D., Labuschagne, C., Langenfelds, R., Laurent, O., Laurila, T., Lauvaux, T., Law, B., Lee, J., Lehner, I., Leuenberger, M., Levin, I., Levula, J., Lin, J., Lindauer, M., Loh, Z., Lopez, M., Luijkx, I. T., Myhre, C. L., Machida, T., Mammarella, I., Manca, G., Manning, A., Manning, A., Marek, M. V., Marklund, P., Martin, M. Y., Matsueda, H., McKain, K., Meijer, H., Meinhardt, F., Miles, N., Miller, C. E., Mölder, M., Montzka, S., Moore, F., Morgui, J.-A., Morimoto, S., Munger, B., Necki, J., Newman, S., Nichol, S., Niwa, Y., O'Doherty, S., Ottosson-Lofvenius, M., Paplawsky, B., Peischl, J., Peltola, O., Pichon, J.-M., Piper, S., Plass-Dolmer, C., Ramonet, M., Reyes-Sanchez, E., Richardson, S., Riris, H., Ryerson, T., Saito, K., Sargent, M., Sasakawa, M., Sawa, Y., Say, D., Scheeren, B., Schmidt, M., Schmidt, A., Schumacher, M., Shepson, P., Shook, M., Stanley, K., Steinbacher, M., Stephens, B., Sweeney, C., Thoning, K., Torn, M., Turnbull, J., Tørseth, K., Bulk, P. V. D., Dinter, D. V., Vermeulen, A., Viner, B., Vitkova, G., Walker, S., Weyrauch, D., Wofsy, S., Worthy, D., Young, D., and Zimnoch, M.: Carbon-Tracker CT2019B, NOAA, <https://doi.org/10.25925/20201008>, 2020.
- King, A. W., Dilling, L., Zimmerman, G. P., Fairman, D. M., Houghton, R. A., Marland, G., Rose, A. Z., Wilbanks, T. J., King, A. W., Dilling, L., Zimmerman, G. P., Fairman, D. M., Houghton, R. A., Marland, G., Rose, A. Z., and Wilbankseditors, T. J.: The first state of the carbon cycle report (SOCCR): The North American carbon budget and implications for the global carbon cycle, U.S. Climate Change Science Program, The first state of the carbon cycle report (SOCCR), The North American carbon budget and implications for the global carbon cycle, 20083154843, xviii + 242 pp., 2007.
- King, A. W., Hayes, D. J., Huntzinger, D. N., West, T. O., and Post, W. M.: North American carbon dioxide sources and sinks: magnitude, attribution, and uncertainty, *Front. Ecol. Environ.*, 10, 512–519, <https://doi.org/10.1890/120066>, 2015.
- Kooijmans, L. M. J., Maseyk, K., Seibt, U., Sun, W., Vesala, T., Mammarella, I., Kolari, P., Aalto, J., Franchin, A., Vecchi, R., Valli, G., and Chen, H.: Canopy uptake dominates nighttime carbonyl sulfide fluxes in a boreal forest, *Atmos. Chem. Phys.*, 17, 11453–11465, <https://doi.org/10.5194/acp-17-11453-2017>, 2017.
- Kuai, L., Parazoo, N. C., Shi, M., Miller, C. E., Baker, I., Bloom, A. A., Bowman, K., Lee, M., Zeng, Z.-C., Commane, R., Montzka, S. A., Berry, J., Sweeney, C., Miller, J. B., and Yung, Y. L.: Quantifying Northern High Latitude Gross Primary Productivity (GPP) Using Carbonyl Sulfide (OCS), *Global Biogeochem. Cy.*, 36, e2021GB007216, <https://doi.org/10.1029/2021GB007216>, 2022.
- LaFranchi, B. W., Pétron, G., Miller, J. B., Lehman, S. J., Andrews, A. E., Dlugokencky, E. J., Hall, B., Miller, B. R., Montzka, S. A., Neff, W., Novelli, P. C., Sweeney, C., Turnbull, J. C., Wolfe, D. E., Tans, P. P., Gurney, K. R., and Guilderson, T. P.: Constraints on emissions of carbon monoxide, methane, and a suite of hydrocarbons in the Colorado Front Range using observations of ¹⁴CO₂, *Atmos. Chem. Phys.*, 13, 11101–11120, <https://doi.org/10.5194/acp-13-11101-2013>, 2013.
- Lauvaux, T., Schuh, A. E., Uliasz, M., Richardson, S., Miles, N., Andrews, A. E., Sweeney, C., Diaz, L. I., Martins, D., Shepson, P. B., and Davis, K. J.: Constraining the CO₂ budget of the corn belt: exploring uncertainties from the assumptions in a mesoscale inverse system, *Atmos. Chem. Phys.*, 12, 337–354, <https://doi.org/10.5194/acp-12-337-2012>, 2012.
- Lauvaux, T., Gurney, K. R., Miles, N. L., Davis, K. J., Richardson, S. J., Deng, A., Nathan, B. J., Oda, T., Wang, J. A., Hutryra, L., and Turnbull, J.: Policy-Relevant Assessment of Urban CO₂ Emissions, *Environ. Sci. Technol.*, 54, 10237–10245, <https://doi.org/10.1021/acs.est.0c00343>, 2020.
- Lehman, S. J., Miller, J. B., Wolak, C., Southon, J., Tans, P. P., Montzka, S. A., Sweeney, C., Andrews, A., LaFranchi, B., Guilderson, T. P., and Turnbull, J. C.: Allocation of Terrestrial Carbon Sources Using ¹⁴CO₂: Methods, Measurement, and Modeling, *Radiocarbon*, 55, 1484–1495, 2013.
- Levin, I., Kromer, B., Schmidt, M., and Sartorius, H.: A novel approach for independent budgeting of fossil fuel CO₂ over Europe by ¹⁴CO₂ observations, *Geophysical Research Letters*, 30, <https://doi.org/10.1029/2003GL018477>, 2003.
- Levin, I. and Karstens, U.: Inferring high-resolution fossil fuel CO₂ records at continental sites from combined ¹⁴CO₂ and CO observations, *Tellus B*, 59, 245–250, <https://doi.org/10.1111/j.1600-0889.2006.00244.x>, 2007.
- Libby, W. F.: Atmospheric Helium Three and Radiocarbon from Cosmic Radiation, *Phys. Rev.*, 69, 671–672, <https://doi.org/10.1103/PhysRev.69.671.2>, 1946.
- Lin, J. C., Gerbig, C., Wofsy, S. C., Andrews, A. E., Daube, B. C., Davis, K. J., and Grainger, C. A.: A near-field tool for simulating the upstream influence of atmospheric observations: The Stochastic Time-Inverted Lagrangian Transport (STILT) model, *J. Geophys. Res.*, 108, 4493, <https://doi.org/10.1029/2002JD003161>, 2003.
- Lopez, M., Schmidt, M., Delmotte, M., Colomb, A., Gros, V., Janssen, C., Lehman, S. J., Mondelain, D., Perrussel, O., Ramonet, M., Xueref-Remy, I., and Bousquet, P.: CO, NO_x and ¹³CO₂ as tracers for fossil fuel CO₂: results from a pilot study in Paris during winter 2010, *Atmos. Chem. Phys.*, 13, 7343–7358, <https://doi.org/10.5194/acp-13-7343-2013>, 2013.
- Ma, J., Rемаud, M., Peylin, P., Patra, P., Niwa, Y., Rodenbeck, C., Cartwright, M., Harrison, J. J., Chipperfield, M. P., Pope, R. J., Wilson, C., Belviso, S., Montzka, S. A., Vimont, I., Moore, F., Atlas, E. L., Schwartz, E., and Krol, M. C.: Intercomparison of Atmospheric Carbonyl Sulfide (TransCom-COS): 2. Evaluation of Optimized Fluxes Using Ground-Based and Aircraft Observations, *J. Geophys. Res.-Atmos.*, 128, e2023JD039198, <https://doi.org/10.1029/2023JD039198>, 2023.

- Maier, F., Rödenbeck, C., Levin, I., Gerbig, C., Gachkivskiy, M., and Hammer, S.: Potential of ¹⁴C-based vs. ΔCO₂-based ΔffCO₂ observations to estimate urban fossil fuel CO₂ (ffCO₂) emissions, *Atmos. Chem. Phys.*, 24, 8183–8203, <https://doi.org/10.5194/acp-24-8183-2024>, 2024a.
- Maier, F., Levin, I., Conil, S., Gachkivskiy, M., Denier van der Gon, H., and Hammer, S.: Uncertainty in continuous ΔCO₂-based ΔffCO₂ estimates derived from ¹⁴C flask and bottom-up ΔCO/ffCO₂ ratios, *Atmos. Chem. Phys.*, 24, 8205–8223, <https://doi.org/10.5194/acp-24-8205-2024>, 2024b.
- Miller, J. B., Lehman, S. J., Montzka, S. A., Sweeney, C., Miller, B. R., Karion, A., Wolak, C., Dlugokencky, E. J., Southon, J., Turnbull, J. C., and Tans, P. P.: Linking emissions of fossil fuel CO₂ and other anthropogenic trace gases using atmospheric ¹⁴CO₂, *J. Geophys. Res.-Atmos.*, 117, D08302, <https://doi.org/10.1029/2011JD017048>, 2012.
- Miller, J. B., Lehman, S. J., Verhulst, K. R., Miller, C. E., Duren, R. M., Yadav, V., Newman, S., and Sloop, C. D.: Large and seasonally varying biospheric CO₂ fluxes in the Los Angeles megacity revealed by atmospheric radiocarbon, *P. Natl. Acad. Sci. USA*, 117, 26681–26687, <https://doi.org/10.1073/pnas.2005253117>, 2020.
- Montzka, S. A., Calvert, P., Hall, B. D., Elkins, J. W., Conway, T. J., Tans, P. P., and Sweeney, C.: On the global distribution, seasonality, and budget of atmospheric carbonyl sulfide (COS) and some similarities to CO₂, *J. Geophys. Res.-Atmos.*, 112, D09302, <https://doi.org/10.1029/2006JD007665>, 2007.
- Oda, T., Maksyutov, S., and Andres, R. J.: The Open-source Data Inventory for Anthropogenic CO₂, version 2016 (ODIAC2016): a global monthly fossil fuel CO₂ gridded emissions data product for tracer transport simulations and surface flux inversions, *Earth Syst. Sci. Data*, 10, 87–107, <https://doi.org/10.5194/essd-10-87-2018>, 2018.
- Pal, S., Davis, K. J., Lauvaux, T., Browell, E. V., Gaudet, B. J., Stauffer, D. R., Obland, M. D., Choi, Y., DiGangi, J. P., Feng, S., Lin, B., Miles, N. L., Pauly, R. M., Richardson, S. J., and Zhang, F.: Observations of Greenhouse Gas Changes Across Summer Frontal Boundaries in the Eastern United States, *J. Geophys. Res.-Atmos.*, 125, e2019JD030526, <https://doi.org/10.1029/2019JD030526>, 2020.
- Parazoo, N. C., Bowman, K. W., Baier, B. C., Liu, J., Lee, M., Kuai, L., Shiga, Y., Baker, I., Whelan, M. E., Feng, S., Krol, M., Sweeney, C., Runkle, B. R., Tajfar, E., and Davis, K. J.: Covariation of Airborne Biogenic Tracers (CO₂, COS, and CO) Supports Stronger Than Expected Growing Season Photosynthetic Uptake in the Southeastern US, *Global Biogeochem. Cy.*, 35, e2021GB006956, <https://doi.org/10.1029/2021GB006956>, 2021.
- Potosnak, M. J., Wofsy, S. C., Denning, A. S., Conway, T. J., Munger, J. W., and Barnes, D. H.: Influence of biotic exchange and combustion sources on atmospheric CO₂ concentrations in New England from observations at a forest flux tower, *J. Geophys. Res.-Atmos.*, 104, 9561–9569, <https://doi.org/10.1029/1999JD900102>, 1999.
- Rastogi, B., Berkelhammer, M., Wharton, S., Whelan, M. E., Iter, M. S., Leen, J. B., Gupta, M. X., Noone, D., and Still, C. J.: Large Uptake of Atmospheric OCS Observed at a Moist Old Growth Forest: Controls and Implications for Carbon Cycle Applications, *Journal of Geophysical Research: Biogeosciences*, 123, 3424–3438, <https://doi.org/10.1029/2018JG004430>, 2018.
- Schuh, A. E., Denning, A. S., Corbin, K. D., Baker, I. T., Uliasz, M., Parazoo, N., Andrews, A. E., and Worthy, D. E. J.: A regional high-resolution carbon flux inversion of North America for 2004, *Biogeosciences*, 7, 1625–1644, <https://doi.org/10.5194/bg-7-1625-2010>, 2010.
- Shiga, Y. P., Michalak, A. M., Gourdji, S. M., Mueller, K. L., and Yadav, V.: Detecting fossil fuel emissions patterns from subcontinental regions using North American in situ CO₂ measurements, *Geophys. Res. Lett.*, 41, 4381–4388, <https://doi.org/10.1002/2014GL059684>, 2014.
- Stein, A. F., Draxler, R. R., Rolph, G. D., Stunder, B. J. B., Cohen, M. D., and Ngan, F.: NOAA's HYSPLIT Atmospheric Transport and Dispersion Modeling System, *Bull. Amer. Meteor. Soc.*, 96, 2059–2077, <https://doi.org/10.1175/BAMS-D-14-00110.1>, 2015.
- Stuiver, M. and Polach, H. A.: Discussion Reporting of ¹⁴C Data, *Radiocarbon*, 19, 355–363, <https://doi.org/10.1017/S0033822200003672>, 1977.
- Sun, W., Maseyk, K., Lett, C., and Seibt, U.: Litter dominates surface fluxes of carbonyl sulfide in a Californian oak woodland, *J. Geophys. Res.-Biogeo.*, 121, 438–450, <https://doi.org/10.1002/2015JG003149>, 2016.
- Sweeney, C., Karion, A., Wolter, S., Newberger, T., Guenther, D., Higgs, J. A., Andrews, A. E., Lang, P. M., Neff, D., Dlugokencky, E., Miller, J. B., Montzka, S. A., Miller, B. R., Masarie, K. A., Biraud, S. C., Novelli, P. C., Crotwell, M., Crotwell, A. M., Thoning, K., and Tans, P. P.: Seasonal climatology of CO₂ across North America from aircraft measurements in the NOAA/ESRL Global Greenhouse Gas Reference Network, *J. Geophys. Res.-Atmos.*, 120, 5155–5190, <https://doi.org/10.1002/2014JD022591>, 2015.
- Sweeney, C., Baier, B. C., Miller, J. B., Lang, P., Miller, B. R., Lehman, S., Michel, S. E., and Yang, M. M.: ACT-America: L2 In Situ Atmospheric Gas Concentrations from Flasks, Eastern USA (Version 1.2), ORNL Distributed Active Archive Center [data set], <https://doi.org/10.3334/ORNLDAAAC/1575>, 2018.
- Tans, P. P., Fung, I. Y., and Takahashi, T.: Observational constraints on the global atmospheric CO₂ budget, *Science*, 247, 1431–1438, <https://doi.org/10.1126/science.247.4949.1431>, 1990.
- Tans, P. P., Berry, J. A., and Keeling, R. F.: Oceanic ¹³C/¹²C observations: A new window on ocean CO₂ uptake, *Global Biogeochem. Cy.*, 7, 353–368, <https://doi.org/10.1029/93GB00053>, 1993.
- Thompson, M. V. and Randerson, J. T.: Impulse response functions of terrestrial carbon cycle models: method and application, *Global Change Biol.*, 5, 371–394, <https://doi.org/10.1046/j.1365-2486.1999.00235.x>, 1999.
- Turnbull, J. C., Miller, J. B., Lehman, S. J., Tans, P. P., Sparks, R. J., and Southon, J.: Comparison of ¹⁴CO₂, CO, and SF₆ as tracers for recently added fossil fuel CO₂ in the atmosphere and implications for biological CO₂ exchange, *Geophys. Res. Lett.*, 33, L01817, <https://doi.org/10.1029/2005GL024213>, 2006.
- Turnbull, J. C., Lehman, S. J., Miller, J. B., Sparks, R. J., Southon, J. R., and Tans, P. P.: A new high precision ¹⁴CO₂ time series for North American continental air, *J. Geophys. Res.-Atmos.*, 112, D11310, <https://doi.org/10.1029/2006JD008184>, 2007.

- Turnbull, J., Rayner, P., Miller, J., Naegler, T., Ciais, P., and Cozic, A.: On the use of ¹⁴CO₂ as a tracer for fossil fuel CO₂: Quantifying uncertainties using an atmospheric transport model, *J. Geophys. Res.*, 114, D22302, <https://doi.org/10.1029/2009JD012308>, 2009.
- Turnbull, J. C., Karion, A., Fischer, M. L., Faloona, I., Guilderson, T., Lehman, S. J., Miller, B. R., Miller, J. B., Montzka, S., Sherwood, T., Saripalli, S., Sweeney, C., and Tans, P. P.: Assessment of fossil fuel carbon dioxide and other anthropogenic trace gas emissions from airborne measurements over Sacramento, California in spring 2009, *Atmos. Chem. Phys.*, 11, 705–721, <https://doi.org/10.5194/acp-11-705-2011>, 2011a.
- Turnbull, J. C., Tans, P. P., Lehman, S. J., Baker, D., Conway, T. J., Chung, Y. S., Gregg, J., Miller, J. B., Southon, J. R., and Zhou, L.-X.: Atmospheric observations of carbon monoxide and fossil fuel CO₂ emissions from East Asia, *J. Geophys. Res.*, 116, D24306, <https://doi.org/10.1029/2011JD016691>, 2011b.
- Turnbull, J. C., Sweeney, C., Karion, A., Newberger, T., Lehman, S. J., Tans, P. P., Davis, K. J., Lauvaux, T., Miles, N. L., Richardson, S. J., Cambaliza, M. O., Shepson, P. B., Gurney, K., Patarasuk, R., and Razlivanov, I.: Toward quantification and source sector identification of fossil fuel CO₂ emissions from an urban area: Results from the INFLUX experiment, *J. Geophys. Res.-Atmos.*, 120, 2014JD022555, <https://doi.org/10.1002/2014JD022555>, 2015.
- Turnbull, J. C., Karion, A., Davis, K. J., Lauvaux, T., Miles, N. L., Richardson, S. J., Sweeney, C., McKain, K., Lehman, S. J., Gurney, K. R., Patarasuk, R., Liang, J., Shepson, P. B., Heimbürger, A., Harvey, R., and Whetstone, J.: Synthesis of Urban CO₂ Emission Estimates from Multiple Methods from the Indianapolis Flux Project (INFLUX), *Environ. Sci. Technol.*, 53, 287–295, <https://doi.org/10.1021/acs.est.8b05552>, 2019.
- USGCRP: Second State of the Carbon Cycle Report, US Global Change Research Program, Washington, D.C., USA, 878, <https://carbon2018.globalchange.gov/> (last access: 5 November 2024), <https://doi.org/10.7930/SOCCR2>, 2018.
- USGCRP: Second State of the Carbon Cycle Report (SOCCR2): A Sustained Assessment Report, edited by: Cavallaro, N., Shrestha, G., Birdsey, R., Mayes, M. A., Najjar, R. G., Reed, S. C., Romero-Lankao, P., and Zhu, Z., U.S. Global Change Research Program, Washington, DC, USA, 878 pp., <https://doi.org/10.7930/SOCCR2.2018>, 2018.
- Vaughn, B. H., Miller, J., Ferretti, D. F., and White, J. W. C.: Stable isotope measurements of atmospheric CO₂ and CH₄, in: *Handbook of Stable Isotope Analytical Techniques*, Elsevier, 272–304, ISBN 978-0-444-51114-0, 2004.
- Vimont, I. J., Turnbull, J. C., Petrenko, V. V., Place, P. F., Karion, A., Miles, N. L., Richardson, S. J., Gurney, K., Patarasuk, R., Sweeney, C., Vaughn, B., and White, J. W. C.: Carbon monoxide isotopic measurements in Indianapolis constrain urban source isotopic signatures and support mobile fossil fuel emissions as the dominant wintertime CO source, *Elementa*, 5, 63, <https://doi.org/10.1525/elementa.136>, 2017.
- Vogel, F., Hamme, S., Steinhof, A., Kromer, B., and Levin, I.: Implication of weekly and diurnal ¹⁴C calibration on hourly estimates of CO₂-based fossil fuel CO₂ data moderately polluted site in southwestern Germany, *Tellus B*, 62, 512–520, <https://doi.org/10.1111/j.1600-0889.2010.00477.x>, 2010.
- Wei, Y., Shrestha, R., Pal, S., Gerken, T., Feng, S., McNelis, J., Singh, D., Thornton, M. M., Boyer, A. G., Shook, M. A., Chen, G., Baier, B. C., Barkley, Z. R., Barrick, J. D., Bennett, J. R., Browell, E. V., Campbell, J. F., Campbell, L. J., Choi, Y., Collins, J., Dobler, J., Eckl, M., Fiehn, A., Fried, A., Digangi, J. P., Barton-Grimley, R., Halliday, H., Klausner, T., Kooi, S., Kostinek, J., Lauvaux, T., Lin, B., McGill, M. J., Meadows, B., Miles, N. L., Nehrir, A. R., Nowak, J. B., Obland, M., O'Dell, C., Fao, R. M. P., Richardson, S. J., Richter, D., Roiger, A., Sweeney, C., Walega, J., Weibring, P., Williams, C. A., Yang, M. M., Zhou, Y., and Davis, K. J.: Atmospheric Carbon and Transport – America (ACT-America) Data Sets: Description, Management, and Delivery, *Earth Space Sci.*, 8, e2020EA001634, <https://doi.org/10.1029/2020EA001634>, 2021.
- Whelan, M. E., Shi, M., Sun, W., Vries, L. K., Seibt, U., and Maseyk, K.: Soil Carbonyl Sulfide (OCS) Fluxes in Terrestrial Ecosystems: An Empirical Model, *J. Geophys. Res.-Biogeo.*, 127, e2022JG006858, <https://doi.org/10.1029/2022JG006858>, 2022.
- Wu, K., Davis, K. J., Miles, N. L., Richardson, S. J., Lauvaux, T., Sarmiento, D. P., Balashov, N. V., Keller, K., Turnbull, J., Gurney, K. R., Liang, J., and Roest, G.: Source decomposition of eddy-covariance CO₂ flux measurements for evaluating a high-resolution urban CO₂ emissions inventory, *Environ. Res. Lett.*, 17, 074035, <https://doi.org/10.1088/1748-9326/ac7c29>, 2022.
- Yang, M. M., Barrick, J. D., Sweeney, C., DiGangi, J. P., and Bennett, J. R.: ACT-America: L1 Meteorological and Aircraft Navigational Data (Version 1.1), ORNL Distributed Active Archive Center [data set], <https://doi.org/10.3334/ORNLDAAAC/1574>, 2018.
- Zazzeri, G., Graven, H., Xu, X., Saboya, E., Blyth, L., Manning, A. J., Chawner, H., Wu, D., and Hammer, S.: Radiocarbon Measurements Reveal Underestimated Fossil CH₄ and CO₂ Emissions in London, *Geophys. Res. Lett.*, 50, e2023GL103834, <https://doi.org/10.1029/2023GL103834>, 2023.
- Zhou, Y., Williams, C. A., Lauvaux, T., Davis, K. J., Feng, S., Baker, I., Denning, S., and Wei, Y.: A Multiyear Gridded Data Ensemble of Surface Biogenic Carbon Fluxes for North America: Evaluation and Analysis of Results, *J. Geophys. Res.-Biogeo.*, 125, e2019JG005314, <https://doi.org/10.1029/2019JG005314>, 2020.